UNIVERSITY OF CALIFORNIA, SAN DIEGO

SEM Analysis of Electrophoretically-Deposited Nanoparticle Films

A thesis submitted in partial satisfaction of the requirements
for the degree Master of Science

in

Chemical Engineering

by

Neil Verma

Committee in charge:

Jan B. Talbot, Chair
Richard K. Herz
Justin P. Opatkiewicz

2015

The Thesis of Neil Verma is approved and it is acceptable in quality and form for publication on microfilm and electronically:

_____

_____

_____

Chair

University of California, San Diego

2015

Dedicated to my loving family

TABLE OF CONTENTS

LIST OF ABBREVIATIONS

CF	Carbon Felt
$CoFe_2O_4$	Cobalt Ferrite
CTAB	Cetyltrimethylammonium bromide
E	Ethanol
EDX	Energy-Dispersive X-Ray Spectroscopy
EPD	Electrophoretic Deposition
gge	Gasoline Gallon Equivalent
GP	Graphite Paper
LSV	Linear Sweep Voltammetry
NHE	Normal Hydrogen Electrode
PEMFC	Polymer Electrolyte Membrane Fuel Cell
Pt_3Co	Platinum Cobalt
SA	Sulfur Ammonia
SCE	Saturated Calomel Electrode
SEM	Scanning Electron Microscope

LIST OF FIGURES

LIST OF TABLES

ACKNOWLEDGEMENTS

I would like to thank Professor Jan B. Talbot for all her support and guidance throughout my undergraduate and graduate studies. Her advice and supervision has played a vital role in my development as a student and researcher. I would also like to thank Professor Richard Herz, Dr. Lloyd Brown, Robin Taylor, and Roger Davenport for all their help and continued support.

This work was funded through a subcontract with SAIC (now leidos), by the Fuel Cell Technologies Office of the U.S. Department of Energy under grant number DE-FG36-07GO17002.

ABSTRACT OF THE THESIS

SEM Analysis of Electrophoretically-Deposited Nanoparticle Films

by

Neil Verma

Master of Science in Chemical Engineering

University of California, San Diego, 2015

Professor Jan B. Talbot, Chair

Cobalt ferrite nanoparticles (20 nm) were synthesized and electrophoretically deposited onto aluminum foil, graphite paper, and carbon felt in order to study its potential as a cost-effective electrocatalyst for the oxidation of ammonium sulfite to ammonium sulfate in a proposed sulfur ammonia thermochemical cycle. Scanning electron microscopy and linear sweep voltammetry were used to characterize the deposited films and investigate their electrochemical activity. Furthermore, the effects of

electrophoretic deposition conditions on deposit morphology and subsequently the effects of deposit morphology on electrochemical activity in 2 M ammonium sulfite were studied to better understand how to improve electrocatalysts. It was found that there is a critical deposit thickness for each substrate, where additional deposited particles reduce overall electrocatalytic activity of the deposits. For graphite paper, this thickness was estimated to be 3 particle layers for the EPD conditions studied. The 3 particle layer film on graphite paper resulted in a 5.5 fold increase in current density from a blank graphite paper substrate. For carbon felt, the deposit thickness threshold was calculated to be 0.13 of a particle layer for the EPD conditions studied. Moreover, this film was found to have a 4.3 fold increase in current density from a blank carbon felt substrate.

Chapter 1. Introduction

Increasing concerns over traditional energy sources in recent years has led to a growing interest in clean, renewable forms of energy. More specifically, tribulations in the transportation sector regarding the volatile price of crude oil and its long-term environmental implications have sparked significant innovation in the efficiency of motor vehicles to mitigate consumption and pollution. Though vast strides have been made in the efficient use of fossil fuels, a long-term sustainable alternative has yet to be successfully integrated into the transportation market.

One alternative to conventional fuel that stands out as a long-term solution is the use of hydrogen in conjunction with fuel cell technology. Similar to refined petroleum, hydrogen can be readily used as a portable means of energy storage [1]. Many benefits can be reaped from the transition to a hydrogen-based automotive industry. For example, using polymer electrolyte membrane fuel cells (PEMFCs) in automobiles on a large-scale would substantially reduce harmful vehicle emissions, as the byproducts produced by PEMFCs are limited to simply water and heat [2]. Additionally, use of hydrogen powered vehicles as a primary mode of transportation could reduce global oil dependence and provide a long-term solution to the depletion of fossil fuel reservoirs.

Though there are many advantages to a hydrogen-driven transportation sector, there is one major caveat to such a solution; hydrogen is not readily available on Earth. Despite being the most abundant element in the universe, elemental hydrogen only exists in minute quantities on earth because the molecules are so light that they mostly escape Earth's gravity [3]. Thus, hydrogen must be chemically derived through various

techniques, including, steam reforming, partial oxidation, and electrolysis [4]. The majority of industrial hydrogen is produced from fossil fuels through the steam reforming or partial oxidation of hydrocarbons [4]. Additionally, hydrogen can be obtained via electrolysis; however, this method poses difficulties in regards to scaling for commercial applications [4]. It is evident that in order to utilize hydrogen as a clean fuel, a cost-effective, renewable means of obtaining hydrogen must be developed.

One potential method for sustainable hydrogen production involves harvesting solar thermal energy to power a water splitting cycle [5]. A sulfur ammonia (SA) thermochemical cycle has been proposed through a U.S. Department of Energy (DOE) funded project for the purpose of constructing a sustainable, cost-effective means of manufacturing hydrogen [6]. The target of this project is to reduce the cost of hydrogen production to $3.00 per gge (gasoline gallon equivalent) by 2017, in order to make hydrogen a viable substitute for gasoline [6]. In order to achieve this goal, operational costs of the SA cycle must be significantly reduced. One substantial cost source that has been identified is the operation of the electrolyzer for the hydrogen producing sub-cycle, due to the kinetically slow, anodic reaction of the oxidation of ammonium sulfite to ammonium sulfate. It is proposed that utilizing electrocatalysts, such as platinum cobalt, could speed up this reaction [6,7]. Despite their effectiveness, platinum-based catalysts are costly for large-scale applications (~$249 per gram) [8]. To reduce costs, cobalt ferrite nanoparticles have been proposed as an inexpensive electrocatalyst (~$13 per gram) for the oxidation of ammonium sulfite [7,9].

The primary motivation of this research was to help in the development of a cost-effective means of producing hydrogen. To achieve this goal, research was conducted to

analyze the use of cobalt ferrite nanoparticles in minimizing electrocatalyst costs for the SA cycle. More specifically, conditions for the deposition of nanoparticles onto various substrates by electrophoretic deposition (EPD) and the resulting deposit morphologies were studied to determine viable ways of manufacturing economical electrodes, thus reducing costs for the proposed SA thermochemical cycle. Furthermore, EPD conditions resulting in thin films were of particular interest, as it was sought to minimize the amount of catalyst needed while exposing the nanoparticles for maximum activity.

The thesis is organized as follows: Chapter 2 provides a brief background on the SA thermochemical cycle, the advantages of nanoparticles as electrocatalysts, and electrophoretic deposition. Chapter 3 describes the experimental procedures used to conduct the research. Chapter 4 contains the findings and implications of the research. Lastly, conclusions and recommendations for future work are laid out in Chapter 5.

References

[1] Perkins, C.; Weimer, A. W. Likely near-term solar-thermal water splitting technologies. *International Journal of Hydrogen Energy*, **2004**, *29*, 1587-1599.

[2] Busby, J.R.; Altork, L. Hydrogen Fuel Cells: Part of the Solution. *Tech. & Eng. Teacher*, **2010**, *70*, 22-27.

[3] Silverberg, M.S. *Principles of General Chemistry*, 2nd ed.; McGraw-Hill: San Diego, CA, 2010, p 434.

[4] Ogden, J.M. Prospects for Building a Hydrogen Energy Infrastructure. *Annu. Rev. Energy Environ.*, **1999**, *24*, 227-279.

[5] Littlefield, J.; Wang, M.; Brown, L.C.; Herz, R.K.; Talbot, J.B. Process Modeling and Thermochemical Experimental Analysis of a Solar Sulfur Ammonia Hydrogen Production Cycle. *Energy Procedia*, **2012**, *29*, 616-623.

[6] Taylor, R.; Davenport, R.; T-Raissi, A.; Muradov, N.; Huang, C.; Fenton, S.; Genders, D.; Symons, P. Solar High-Temperature Water-Splitting Cycle with Quantum Boost. *DOE Hydrogen Program: FY 2010 Annual Progress Report.* **2010**, 120-125.

[7] Tanakit, R.; Luc, W.; Talbot, J.B. Electrophoretic Deposition of Cobalt Ferrite and Platinum Cobalt Nanoparticles as Electrocatalysts. *ECS Transactions*. **2014**, *58*, 1-9.

[8] Sigma Aldrich. *Platinum cobalt on carbon*; http://www.sigmaaldrich.com/catalog/product/aldrich/738565?lang=en&region=US, Product No. 738565.

[9] Sigma Aldrich. *Cobalt Iron Oxide*; http://www.sigmaaldrich.com/catalog/product/aldrich/773352?lang=en&region=US, Product No. 773352.

Chapter 2. Background

2.1 Solar Sulfur Ammonia Thermochemical Cycle

A thermochemical cycle is a water-splitting method that combines heat with chemical processes to produce hydrogen and oxygen [1]. The sulfur ammonia (SA) thermochemical cycle studied in this research, shown in Figure 2.1, was originally developed by the Florida Solar Energy Center [2]. The chemical reactions of the SA cycle are summarized in the following steps [3]:

(1) $SO_2\ (g) + 2NH_3\ (g) + \mathrm{H_2O}\ (l) \rightarrow (NH_4)_2\mathrm{SO_3}\ (aq)$ (298-323 K)

(2) $(NH_4)_2\mathrm{SO_3}\ (aq) + \mathrm{H_2O}\ (l) \rightarrow (NH_4)_2\mathrm{SO_4}\ (aq) + \mathbf{H_2}\ (\boldsymbol{g})$ (353-423 K)

(3) $(NH_4)_2\mathrm{SO_4}\ (aq) + K_2\mathrm{SO_4}\ (l) \rightarrow 2NH_3\ (g) + K_2S_2\mathrm{O_7}\ (l) + \mathrm{H_2O}\ (g)$ (673-723 K)

(4) $K_2S_2\mathrm{O_7}\ (l) \rightarrow \mathrm{SO_3}\ (g) + K_2\mathrm{SO_4}\ (l)$ (1063 K)

(5) $\mathrm{SO_3}\ (g) \rightarrow\ SO_2\ (g) + \frac{1}{2}\boldsymbol{O_2}\ (\boldsymbol{g})$ (1123-1473 K)

The electrolytic oxidation of ammonium sulfite to ammonium sulfate in step (2) produces hydrogen gas and occurs at above ambient temperature and reasonably low pressures [3]. A sub-cycle is created by steps (3)-(4) in which potassium sulfate and ammonium sulfate react in the low-temperature reactor to produce potassium pyrosulfate [3]. Subsequently, the potassium pyrosulfate is fed into the medium temperature reactor, where it decomposes to sulfur trioxide and potassium sulfate, thus closing the sub-cycle [3]. Oxygen is produced in step (5), which occurs at high temperatures over a catalyst [3]. The separation of oxygen from SO_2 occurs in step (1), where SO_2 and NH_3 are chemically absorbed into water [3]. The net result of steps (1)-(5) is the decomposition

of water to form hydrogen and oxygen. It should be noted that all species are recycled in this cycle with the exception of the produced hydrogen and oxygen.

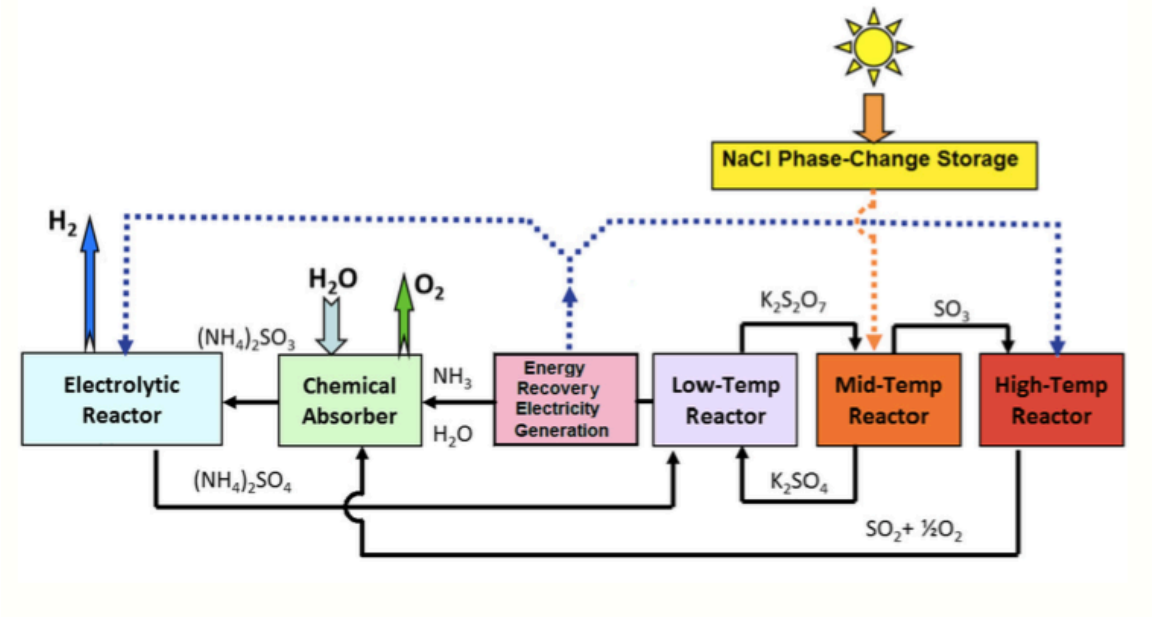

Figure 2.1: Schematic of the sulfur ammonia thermochemical cycle [3]

The hydrogen-producing step in the SA cycle can be separated into its anodic and cathodic reactions as follows [4]:

Anode: $SO_3^{2-} + 2OH^- \rightarrow SO_4^{2-} + H_2O + 2e^-$ E° = -0.936 V

Cathode: $2H_2O + 2e^- \rightarrow H_2 + 2OH^-$ E° = -0.828 V

Overall: $SO_3^{2-} + H_2O \rightarrow SO_4^{2-} + \mathbf{H_2}$ $E°_{cell}$ = 0.108 V

Electrocatalysts are being sought to improve the kinetically slow anodic reaction [4]. It has been proposed that electrocatalysts, such as platinum cobalt, could speed up this reaction; however, due to the cost of platinum, cobalt ferrite nanoparticles were studied as an inexpensive alternative for industrial use [4,5]. Furthermore, nanoparticle electrocatalysts have exhibited potential in reducing costs due to quantum confinement effects and increased catalyst surface area, thus allowing for a greater utilization of

materials [4,6]. In addition, studies have shown cobalt ferrite nanoparticles to be suitable for electrophoretic deposition [4,7].

2.2 Electrophoretic Deposition

2.2.1 Electrophoretic Deposition Overview

Electrophoretic deposition (EPD) is a highly versatile technique used for depositing particles suspended in a liquid medium onto a conductive substrate through the application of an electric field. EPD has become an increasingly popular method in both academia and industry due to its simplicity and relatively low costs [8]. There are two different types of EPD, which depends on whether particles are deposited on the cathode or the anode [8]. If the particles are positively charged, deposition occurs on the cathode (cathodic EPD), whereas if the particles are negatively charged, deposition occurs on the anode (anodic EPD), as shown in Figure 2.2 [8].

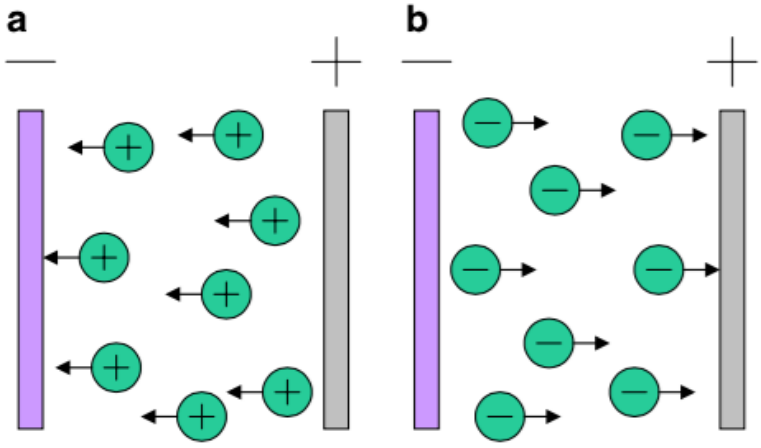

Figure 2.2: Schematic of EPD process (a) cathodic EPD (b) anodic EPD [8]

The primary driving force for EPD is the charge on the particles and the electrophoretic mobility of the particles in the solvent, influenced by the applied electric

field [8]. An electrical double layer is formed at the solid/liquid interface a particle due to the columbic interaction between the particle surface and surrounding oppositely charged ions [9]. Figure 2.3 shows a positively charged particle with a negatively charged double layer. Both the particle and its electrical double layer are located within the shear plane [9]. The diffuse layer surrounds the shear plane and is comprised of negatively and positively charged particles. The potential difference between the shear plane and the diffuse layer is called the zeta potential [8].

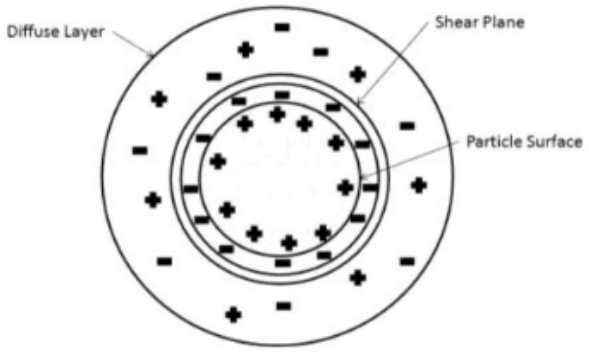

Figure 2.3: Electrical double layer around a spherical particle [9]

2.2.2 Zeta Potential

Zeta potential provides information regarding the intensity of the repulsive interaction between particles and thus the overall stability of a suspension [8]. A large electrostatic repulsion between particles, due to high particle charge, is desired to avoid particle agglomeration [8]. Moreover, a high surface charge during EPD will cause particles to repulse each other, occupying positions which can help lead to a higher particle packing density [8]. Zeta potential can be altered through the addition of charging agents such as acids, bases, or salts to the suspending solution [9]. Zeta

potential measurements to determine the optimal pH for suspension stability of the solutions studied in this research were performed by Nicole Pacheco [10].

Additionally, zeta potential is used in determining electrophoretic velocity [8]. The electrophoretic velocity can be calculated from the Smoluchowski equation, as follows:

$$v = \frac{\xi \varepsilon E}{\eta}$$

where v is the electrophoretic velocity, ξ is the zeta potential, ε is the dielectric constant of the liquid, E is the applied electric field, and η is the viscosity of the liquid [9]. The applied electric field (E) is proportional to deposition current. Once the electrophoretic velocity has been determined, the theoretical deposition mass can be calculated using the Hamaker equation:

$$m = CvAt$$

where m is the deposition mass, C is the suspension concentration, v is the electrophoretic velocity, A is the deposition area, and t is the deposition time [9].

2.2.3 EPD Variations

Figure 2.4 shows a plot of weight-fraction deposited as a function of time for four different deposition conditions [11]. Curve I (constant deposition current, constant suspension concentration) follows the linear relationship expected from the Hamaker equation [11]. Curve II (constant deposition current, varied suspension concentration), curve III (constant voltage, constant suspension concentration), and curve IV (constant voltage, varied suspension concentration) all deviate from the linearity exhibited by curve I. The decline in deposited weight for curve II occurs as a result of decreased particle

concentration in the suspension [11]. For curve III (constant voltage), the deviation from the linear relationship occurs as a result of the decrease in particle velocity, due to increasing deposit resistance with time [11]. Curve IV deviates the most from curve I as a result of the combined effects of decreased concentration and increased deposit resistance [11]. The depositions analyzed in this thesis use a constant deposition current as opposed to a constant deposition voltage.

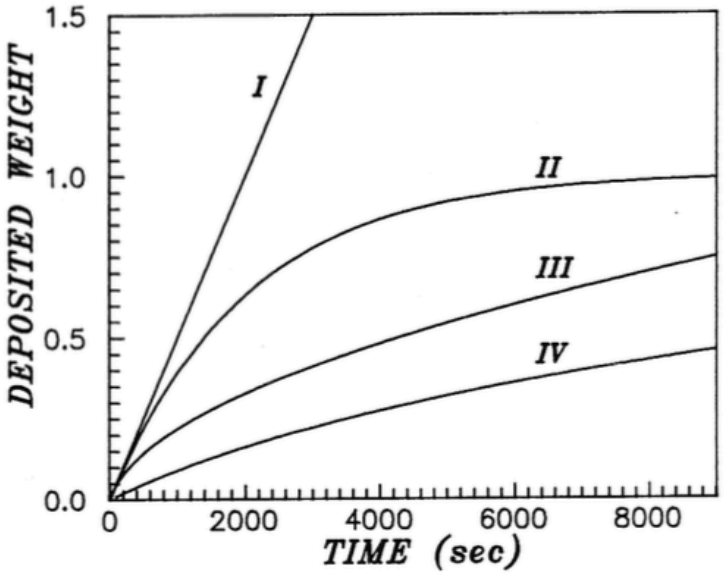

Figure 2.4: Plot of deposited weight as a function of time for different deposition conditions (curve I: constant current/constant concentration; curve II: constant current/variable concentration; curve III: constant voltage/constant concentration, curve IV: constant voltage/variable concentration) [11]

2.2.4 EPD from an Ethanol Bath

Prior work from our group included the EPD of cobalt ferrite using different bath chemistries [4,10]. The different baths included: a 100% ethanol bath and a 90/10 vol. % water/isopropanol bath with either 0.05 mM or 1mM CTAB [10]. It was determined via scanning electron microscope (SEM) analysis that the ethanol bath produced more reproducible deposits than the other baths. Furthermore, calculations showed that EPD of

the cobalt ferrite nanoparticles from the ethanol bath would be able to penetrate 3D substrates [10]. Thus, EPD using a 100% ethanol bath was used in this study.

2.3 Linear Sweep Voltammetry

Linear sweep voltammetry (LSV) typically involves a three-electrode setup, consisting of a working electrode, a reference electrode, and a counter electrode. The working electrode is where the electrochemical reaction takes place [12]. The reference electrode is always at a known potential and serves as a means for measuring the potential drop between it and the working electrode [12]. The counter electrode is used to provide current needed for the reactions on the working electrode [12]. In LSV, current is measured at the working electrode, while the potential between the reference and working electrode is varied at a constant rate [12]. Typically, linear sweep voltammograms plot the applied potential on the x-axis and the resulting current on the y-axis [12]. As potential is increased, the reaction shifts from equilibrium at the surface of the working electrode, causing current to flow. The measured current provides the rate at which electrons transfer at the electrode/electrolyte interface [12]. Thus, currents can be compared for different working electrodes to determine the overall rate of oxidation or reduction.

References

[1] Idaho National Laboratory. Producing Hydrogen: The Thermochemical Cycles.

[2] T-Raissi, A.; Muradov, N.; Huang, C.; Adebiyi, O. Hydrogen from solar via light-assisted high-temperature water splitting cycles. *Journal of Solar Energy Engineering*. **2007**, *129*, 184-189.

[3] Taylor, R.; Davenport, R.; Talbot, J.B.; Herz, R.; Luc, W.; Genders, D.; Symons, P.; Brown, L. Status of the solar sulfur ammonia thermochemical hydrogen production system for splitting water. *Energy Procedia*, **2014**, *49*, 2047-2058.

[4] Tanakit, R.; Luc, W.; Talbot, J.B. Electrophoretic Deposition of Cobalt Ferrite and Platinum Cobalt Nanoparticles as Electrocatalysts. *ECS Transactions*. **2014**, *58*, 1-9.

[5] Taylor, R.; Davenport, R.; T-Raissi, A.; Muradov, N.; Huang, C.; Fenton, S.; Genders, D.; Symons, P. Solar High-Temperature Water-Splitting Cycle with Quantum Boost. *DOE Hydrogen Program: FY 2010 Annual Progress Report.* **2010**, 120-125.

[6] Teranishi, T.; Hosoe, M.; Tanaka, T.; Miyake, M. Size Control of Monodispersed Pt Nanoparticles and Their 2D Organization by Electrophoretic Deposition. *The Journal of Physical Chemistry*. **1999**, *103*, 3818-3827.

[7] Jian, G.; Lu, S.; Zhou, D.; Yang, J.; Fu, Q. Cobalt ferrite dispersion in organic solvents for electrophoretic deposition: Influence of suspension parameters on the film microstructure. *Materials Chemistry and Physics*. **2014**, *143*, 653-660.

[8] Besra, L.; Liu, M. A review on fundamentals and applications of electrophoretic deposition (EPD). *Progress in Materials Science*, **2007**, *52*, 1-61.

[9] Luc, W.; Synthesis and Electrophoretic Deposition of Cobalt Ferrite Nanoparticles. **2012**.

[10] Pacheco, N.S. Electrophoretic Deposition of Cobalt Ferrite Nanoparticles into 3D Felt. M.S. Thesis, University of California, San Diego, 2015.

[11] Sarkar, P.; Nicholson, P.S. Electrophoretic Deposition (EPD): Mechanisms, Kinetics, and Application to Ceramics. *Journal of the American Ceramic Society*, **1996**, *79*, 1987-2002.

[12] Princeton Applied Research. A Review of Techniques for Electrochemical Analysis. *Application Note E-4*.

Chapter 3. Experimental

3.1 Nanoparticle Synthesis

Cobalt ferrite nanoparticles were synthesized by the following co-precipitation reaction [1]:

$$Co^{2+}\ (aq) + 2Fe^{3+}\ (aq) + 8OH^{-}\ (aq) \rightarrow \mathbf{CoFe_2O_4}\ (\boldsymbol{s}) + 4H_2O\ (aq)$$

A 20 ml solution of 0.68 M NaOH was heated to 80 ± 1°C under constant stirring. Once the solution reached 80°C, a 40 mL mixture composed of 20 mL $Co(CH_3COO)_2{\cdot}4H_2O$ (0.085 M) and 20 mL $Fe(NO_3)_3{\cdot}9H_2O$ (0.17 M) was poured into the NaOH solution. The resulting mixture was heated to and maintained at 100 ± 1°C for two hours to allow for the formation of the spherical nanoparticles. The mixture was then allowed to cool to room temperature and washed twice with 200 mL of distilled water to remove contaminants from the solution. These particles were then washed once more with a 100% ethanol solution, prior to addition to the final ethanol bath. A cylindrical neodymium magnet (2.5 cm diameter) was used to separate the magnetic cobalt ferrite nanoparticles from the washing solution. After washing, the cobalt ferrite nanoparticles were placed into 200 mL of 100% ethanol to make a 2 g/L cobalt ferrite ethanol bath for subsequent electrophoretic deposition.

Platinum cobalt nanoparticles loaded on carbon, purchased from Sigma Aldrich, were similarly put into 200 mL of 100% ethanol to make a 2 g/L platinum cobalt ethanol bath for comparison to the cobalt ferrite ethanol bath mentioned. Information regarding the platinum cobalt particles is listed in the Appendix (Figure A.1).

3.2 Electrophoretic Deposition

In order to keep the nanoparticles in suspension for EPD, the pH of the ethanol baths were reduced from 8.0 ± 0.1 to 5.0 ± 0.1 with the addition of nitric acid [2,3]. The pH was measured using an Orion model SA 720 pH meter. To maintain a constant pH, each bath was covered with a nitrogen blanket and the container carefully sealed with paraffin after each use.

The cobalt ferrite and platinum cobalt nanoparticles were electrophoretically deposited on three different substrates: aluminum foil, graphite paper, and carbon felt (3 mm thickness). Information regarding the substrates is listed in the Appendix (Figures A2-A3). Prior to deposition, each bath was sonicated using a Branson 1200 sonicator for ten minutes to reduce particle agglomeration in the suspension. Experiments were conducted to determine the effectiveness of constant sonication compared to constant stirring of the baths throughout the deposition process (Chapter 4). It was determined that initial sonication prior to constant stirring with a magnetic stir-bar (medium speed) during EPD was best for deposit uniformity; thus, sonication followed by continuous stirring of the ethanol baths was utilized in all depositions.

Two different setups were used for the EPD process (Figure 3.1). The first setup in Figure 3.1a was utilized for deposition on aluminum and graphite paper substrates, such that the particles deposited on only one side of substrate. The second setup in Figure 3.1b was used for depositions on the 3 mm carbon felt substrates. For carbon felt substrates, particles were deposited on both sides of the sample in order to maintain deposit uniformity and increase particle penetration towards the middle of the substrate. Both setups utilized a parallel-plate configuration in which a 15 cm^2 aluminum anode

was placed 2 cm from the intended deposition surface (substrate). Furthermore, substrates were held between two insulating Teflon plates with specified areas cut out to expose the substrate surface for deposition. The deposition area for aluminum and graphite paper substrates was 3.14 cm^2, while the deposition region for carbon felt substrates was 1 cm^2 on each side of the sample.

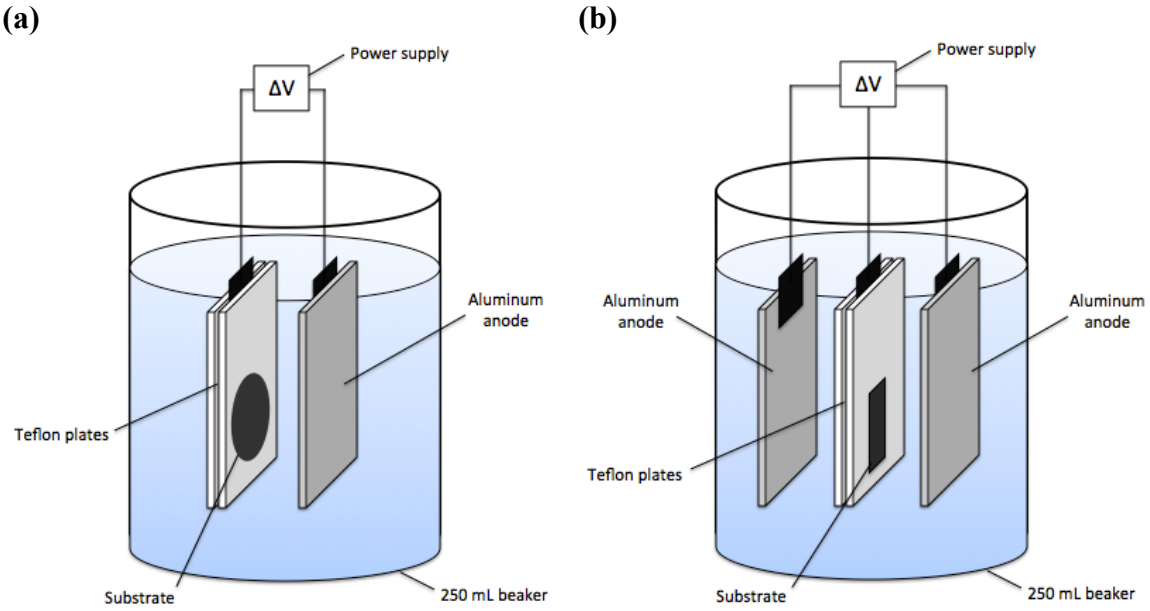

Figure 3.1: Different EPD setups for: (a) aluminum & graphite paper substrates (b) 3 mm carbon felt substrates

To perform the EPD process, a constant current was applied between the aluminum anode(s) and the substrate (cathode) in the nanoparticle suspensions. Deposition current (0-16 mA) and deposition time (0-10 minutes) were varied to study the changes in deposit morphologies as a result of different EPD conditions. Dip-coating tests were also performed, where the substrate was dipped in the nanoparticle suspension (no deposition current) and immediately removed to see if particles deposited. After the deposition process, samples were baked in a vacuum oven (NAPCO - Model 5831) at

200°C to increase deposit adhesion and allow for reliable weight measurements by evaporating any excess ethanol remaining on the samples. In order to determine the weight of deposited nanoparticles on a sample, each sample was weighed before and after the EPD process. All deposit weight measurements were within a ± 0.02 mg error range.

After the completion of the EPD process, samples were prepared for electrochemical testing by soaking the samples in 2 M ammonium sulfite for 24 hours to increase reproducibility. This soaking process ensured that the entirety of each sample was wetted with the ammonium sulfite solution.

3.3 Sample Characterization

3.3.1 Electrochemical Testing

Following EPD and the 24 hour soaking period, the samples were tested for electrocatalytic activity in a standard three-electrode system (Figure 3.2) with 2 M ammonium sulfite. An 8 cm^2 piece of graphite cloth was used as a counter electrode, while a standard calomel electrode (SCE) was used as the reference electrode. The EPD sample was the working electrode in this setup. The areas used for graphite paper and carbon felt samples were 3.14 cm^2 and 1 cm^2, respectively.

Linear sweep voltammetry (LSV) was conducted from 0.0 V to 1.0 V vs. NHE at a scan rate of 50 mV/s using a Princeton Applied Research VersaSTAT 3 potentiostat. In order to determine the effectiveness of samples in improving the ammonium sulfite to ammonium sulfate reaction, the measured current densities of EPD samples were compared to ‘blank’ samples (the substrate only). All current densities were compared at an applied voltage of 0.9 V.

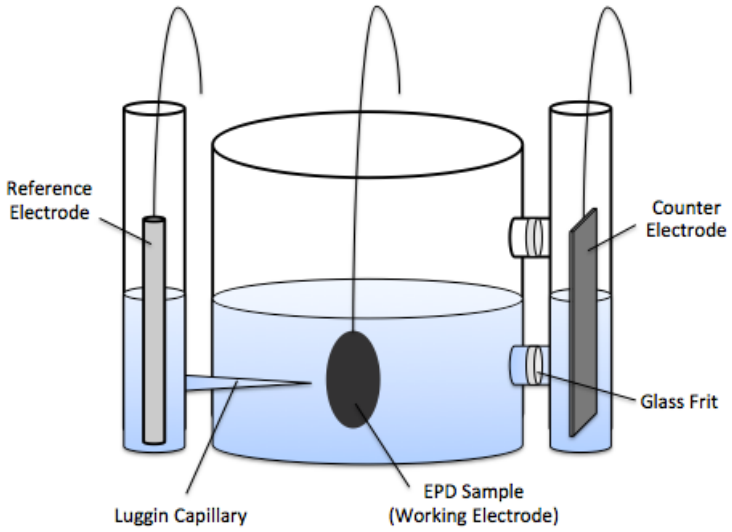

Figure 3.2: Standard three-electrode system used in electrochemical tests

3.3.2 SEM and EDX Analyses

To confirm the composition of the synthesized particles, the particle suspensions were sonicated and samples of each solution were placed drop-wise onto an aluminum substrate for analysis. The nanoparticle composition was then determined utilizing energy-dispersive x-ray spectroscopy (EDX) along with Inca software.

A Phillips XL30 ESEM scanning electron microscope (SEM) with an Oxford Instruments EDX attachment (Model 6650) was used to analyze samples of the deposited films. Samples that had been previously used in electrochemical testing were rinsed thoroughly with deionized water to remove any ammonium sulfate covering the surface of the samples; otherwise, untested samples remained untreated when taking SEM images. Measurement software was used in conjunction with a SEM in order to obtain values for particles size and deposit thickness from high-resolution micrographs. Deposit thicknesses were measured via cross-section SEM analysis, when applicable. In general,

depth of focus was used to approximate relative deposit thickness variations in the acquisition of top-down SEM images.

References

[1] Zi, Z.; Sun, Y.; Zhu, X.; Yang, Z.; Dai, J.; Song, W. Synthesis and magnetic properties of $CoFe_2O_4$ ferrite nanoparticles. *Journal of Magnetism and Magnetic Materials*. **2009**, *321*, 1251-1255.

[2] Tanakit, R.; Luc, W.; Talbot, J.B. Electrophoretic Deposition of Cobalt Ferrite and Platinum Cobalt Nanoparticles as Electrocatalysts. *ECS Transactions*. **2014**, *58*, 1-9.

[3] Pacheco, N.S. Electrophoretic Deposition of Cobalt Ferrite Nanoparticles into 3D Felt. M.S. Thesis, University of California, San Diego, 2015.

Chapter 4. Results and Discussion

4.1 Nanoparticle Characterization

The composition of the synthesized $CoFe_2O_4$ particles was found to be 8.18 at. % Co, 15.53 at. % Fe, and 45.89 at. % O using EDX, corresponding to an atomic ratio of 1:1.9:5.6 (Co:Fe:O) or $CoFe_2O_6$. The extra oxygen measured was most likely a result of oxygen adsorption on the surface of the aluminum substrate. After verifying of the composition, average particle diameter of the cobalt ferrite nanoparticles was measured from an SEM image to be 22 ± 3 nm.

Likewise, the purchased platinum cobalt particles were characterized using EDX and found to have a composition of 1.25 at. % Pt and 0.42 at. % Co, resulting in an atomic ratio of 3:1 ratio of Pt:Co or Pt_3Co. Furthermore, the average diameter of the platinum cobalt on carbon particles was measured from an SEM image to be 50 ± 6 nm. The size of the Pt_3Co by itself could not be determined via SEM analysis.

4.2 EPD on Aluminum Substrates

4.2.1 Deposit Uniformity

The synthesized cobalt ferrite nanoparticles were initially deposited on aluminum foil substrates to investigate the effects of EPD conditions on deposit morphology. Since deposit morphology may significantly alter the electrocatalytic activity of the samples, experiments were first conducted to explore potential means of obtaining reproducible and uniform deposits. Three variations of suspension agitation during EPD were investigated: EPD with constant sonication (without stirring), EPD with constant stirring

(without sonication), and EPD with both sonication and stirring. An intermediate deposition current of 8 mA and deposition time of 2 minutes was selected to perform these depositions. After completing the EPD process, the samples were examined under an SEM to analyze deposit uniformity for each sample. The sample deposit weights for the three EPD agitation cases are shown in Table 4.1.

Figure 4.1 shows the deposit morphology (compared to a blank substrate) for each of the different agitation conditions listed in Table 4.1. Using sonication alone led to localized deposits, as shown in Figure 4.1b. This effect could be a result of the particles settling during the EPD process, leading to different particle concentrations throughout the bath. For constant stirring, deposition uniformity was significantly enhanced compared to sonication; however, slight irregularities were still apparent, as shown in Figure 4.1c. In order test the combined effects of sonication and stirring on the EPD process, the cobalt ferrite ethanol bath was first sonicated for 10 minutes prior to EPD; then, during EPD, the bath was constantly stirred. This method proved to be the most effective in producing consistent, uniform samples, as shown in Figure 4.1d. The uniform deposits most likely result from a reduction in particle agglomeration due to sonication prior to deposition, combined with the constant stirring of the particle suspension (decreasing particle settling in the bath). Therefore, it was determined that sonication prior to EPD with constant stirring led to more uniform deposits compared to either sonication or stirring alone.

Table 4.1: Resulting deposit weight for EPD on aluminum (3.14 cm^2 deposition area) at deposition current of 8 mA and deposition time of 2 min for various particle suspension agitations

Agitation	Deposited Weight (mg)
Sonication	0.36
Stirring	0.43
Combined	0.49

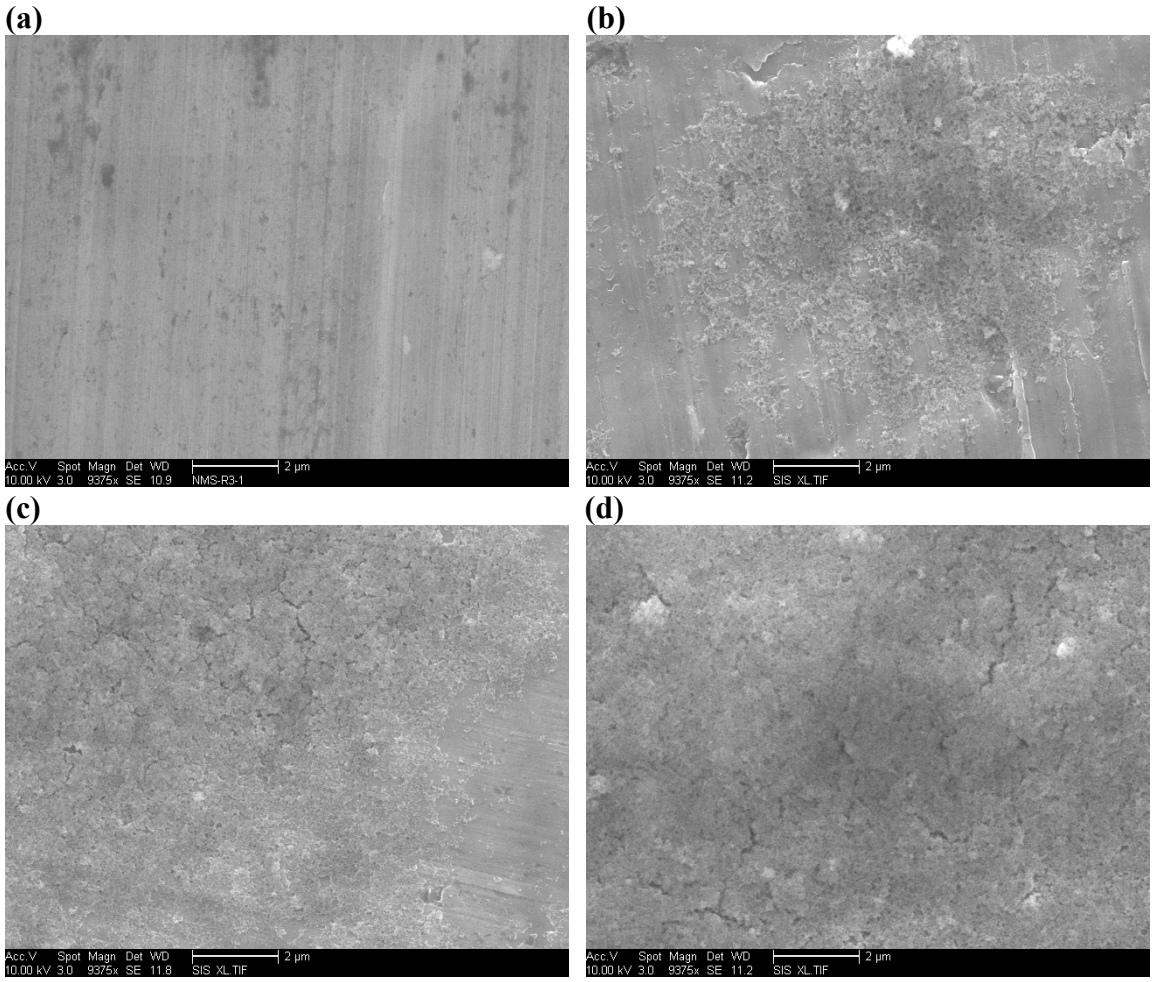

Figure 4.1: SEM micrographs of (a) blank aluminum substrate and EPD deposits at a constant current of 8 mA, time of 2 minutes with (b) sonication (c) stirring (d) combined

4.2.2 Constant Deposition Time

To gain a better understanding of the effect of EPD conditions on deposit morphology, two sets of depositions were performed on aluminum substrates. The first set of depositions included five samples and was conducted at a constant intermediate current of 8 mA, while deposition time was varied for each sample from 30 seconds to 10 minutes (Table 4.2). It was observed that as deposition time was increased, deposition weight also increased, as expected (Figure 4.2). The dip-test data point was measured to have no deposit weight. The data in Figure 4.2 does not satisfy the Hamaker equation, as deposit weight does not increase linearly from the measured dip-test deposit weight of zero milligrams.

Figure 4.3 shows SEM micrographs detailing the changes in deposit morphology as deposition time was varied. Sample 1 (30 seconds deposition time, 0.25 mg deposit weight) has a relatively sparse amount of cobalt ferrite deposited on the surface of the aluminum substrate (Figure 4.3b). There are regions where patches of a thin deposit are observed; however, a vast amount of the surface remained free of deposit. In contrast, Sample 3 (2 minutes deposition time, 0.46 mg deposit weight) has less exposed aluminum, as a result of greater deposit coverage, as shown in Figure 4.3c. Despite this difference, Sample 3 appears to have a similar deposit thickness compared to Sample 1. Sample 5 (10 minutes deposition time, 0.92 mg deposit weight) had the largest amount of deposited cobalt ferrite of this set of experiments and similarly shows the greatest deposit coverage in Figure 4.3d. The nanoparticles are deposited more uniformly on Sample 5 compared to other samples in this set. Moreover, the deposit thickness is noticeably thicker than the more localized deposits at lower deposition times. As shown in Figure

4.3, there is a stark difference in deposit morphology between Samples 1 and 5. Sample 5 had nearly a four-fold increase in deposited weight compared to Sample 1, and the deposit thickness was enough for cracking to occur in the cobalt ferrite deposition layer.

Table 4.2: Deposit weight for EPD on aluminum (3.14 cm^2 deposition area) at a deposition current of 8 mA for various deposition times

Sample Number	Deposition Time (min)	Deposited Weight (mg)
Blank	0.0	0.00
1	0.5	0.25
2	1.0	0.32
3	2.0	0.46
4	5.0	0.67
5	10.0	0.92

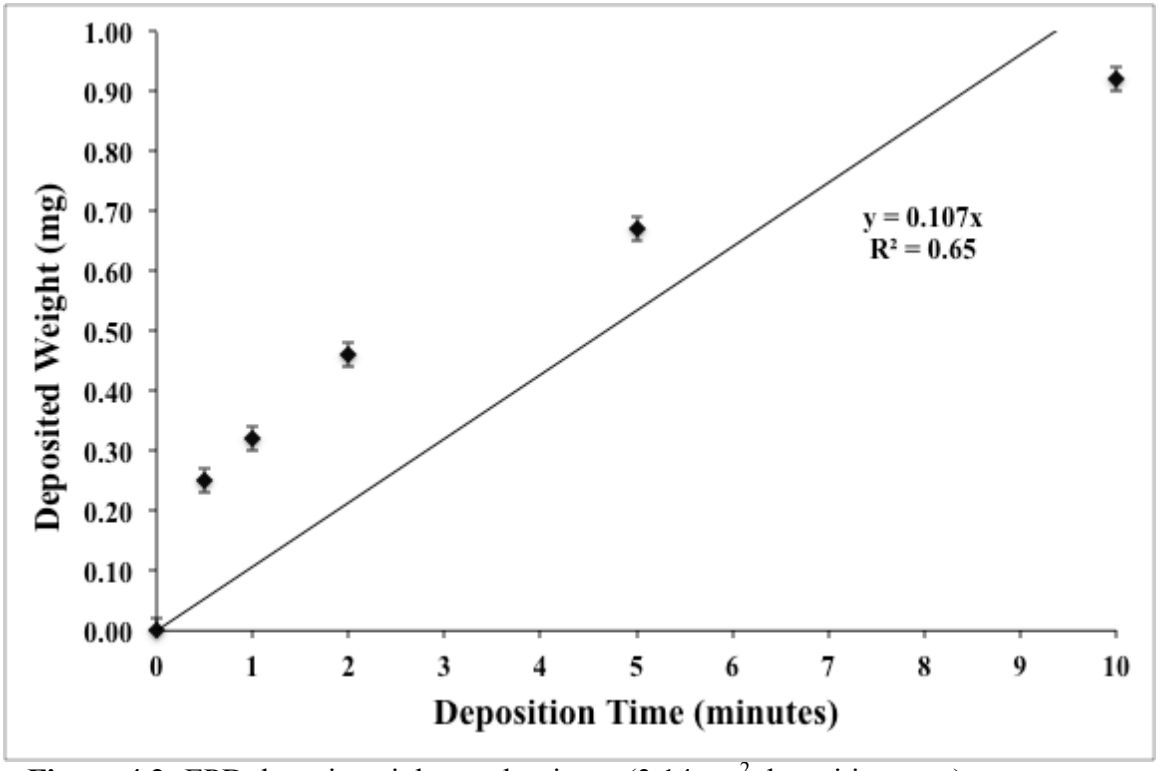

Figure 4.2: EPD deposit weight on aluminum (3.14 cm^2 deposition area) at a constant deposition current of 8 mA for various deposition times

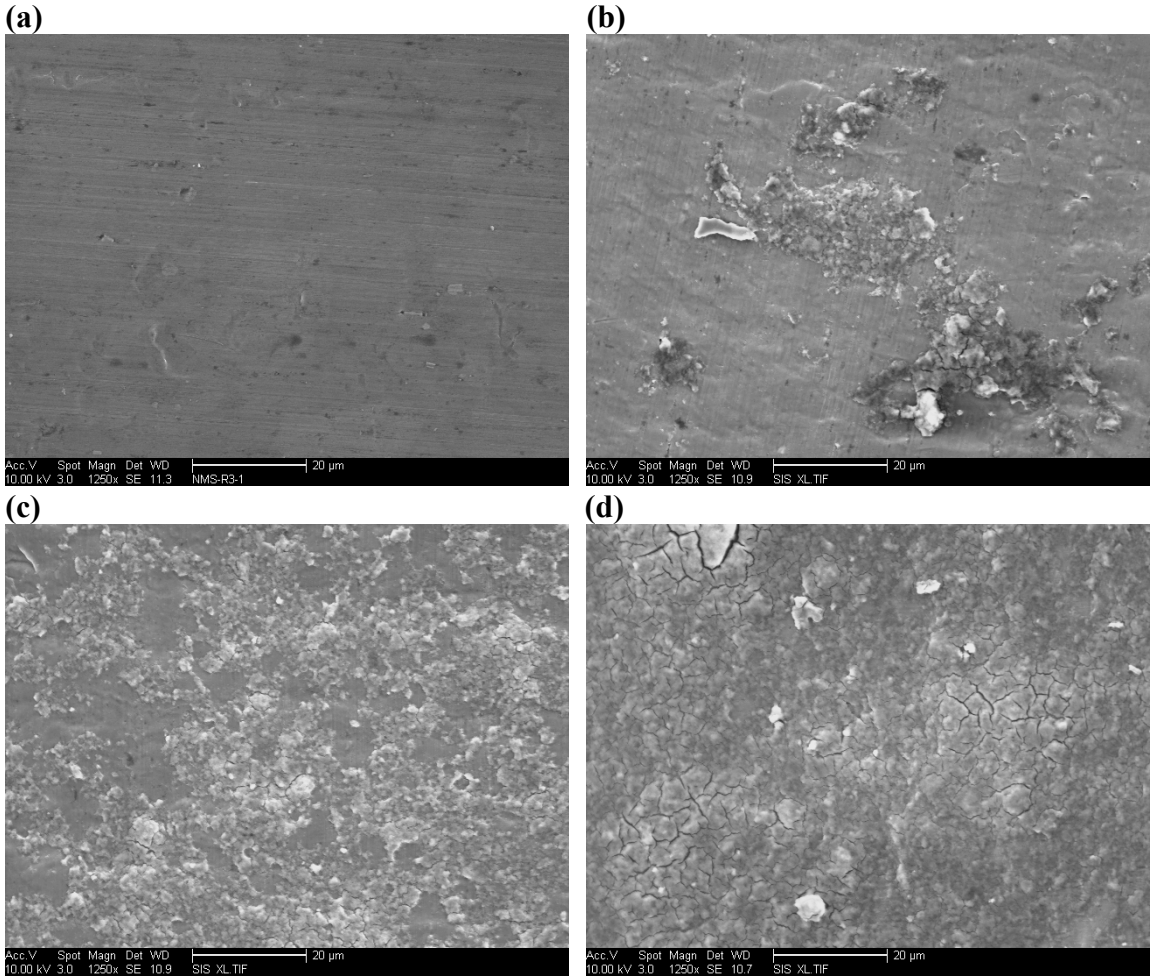

Figure 4.3: SEM micrographs of (a) blank aluminum substrate and EPD deposits at a constant current of 8 mA, time of (b) 30 seconds (c) 2 minutes (d) 10 minutes

4.2.3 Constant Deposition Current

In order to explore the influence of deposition current on deposit morphology for deposits on aluminum, additional tests were performed where deposition time was held constant, and deposition current was varied. The deposition time was held constant at 2 minutes, while deposition current was varied from 2-16 mA in 2 mA increments. Table 4.3 shows the EPD conditions of each sample in this data set and the corresponding deposit weight. As deposition current was increased, deposited weight increased in a relatively linear manner, as shown in Figure 4.4.

SEM micrographs of deposits on aluminum for the various currents are shown in Figure 4.5. Sample 6 (2 mA deposition current, 0.18 mg deposit weight) has a thin, sparse layer of cobalt ferrite deposited on the aluminum substrate (Figure 4.5b). As deposition current was increased, deposit thickness began to increase as shown in the SEM image for Sample 10 (10 mA deposition current, 0.69 mg deposit weight) in Figure 4.5c. Sample 10 has regions of thin, sparse cobalt ferrite deposit, in addition to well-covered, thicker deposit regions with slight cracking. When the deposition current was increased even further, deposit cracking becomes more noticeable. Sample 13 (16 mA deposition current, 1.20 mg deposit weight) is fully coated with the cobalt ferrite and significant deposit cracking is observed in Figure 4.5d.

Similar to the deposits from varied deposition time on aluminum, the samples from varying deposition current also displayed significant differences in deposit morphology as deposit weight increased. Increases in deposition current resulted in more particles deposited onto the aluminum substrate and thus greater deposit coverage; moreover, deposit thickness was increased as well as deposit cracking.

In order to approximate the magnitude of deposit thickness achieved with larger deposit weights, calculations were performed to estimate the number of particle layers present, assuming hexagonal close packing. The mass of a monolayer per cm^2 of the 20 nm cobalt ferrite nanoparticles was determined to be 10.2 $\mu g/cm^2$ [1]. For the substrate area of 3.14 cm^2 on aluminum, the deposit weight for a monolayer was calculated to be 0.032 mg [1]. Sample 13 had a deposit weight of 1.20 mg; therefore, if the deposit was uniform throughout and fully covered the aluminum substrate, there would be approximately 30 layers present. The substantial cracking observed in Figure 4.5d suggests that there are many layers present, agreeing with the calculated result.

Table 4.3: Deposit weight for EPD on aluminum (3.14 cm^2 deposition area) at a deposition time of 2 minutes for various deposition currents

Sample Number	Deposition Current (mA)	Deposited Weight (mg)
Blank	0	0.00
6	2	0.18
7	4	0.24
8	6	0.43
9	8	0.49
10	10	0.69
11	12	0.92
12	14	1.09
13	16	1.20

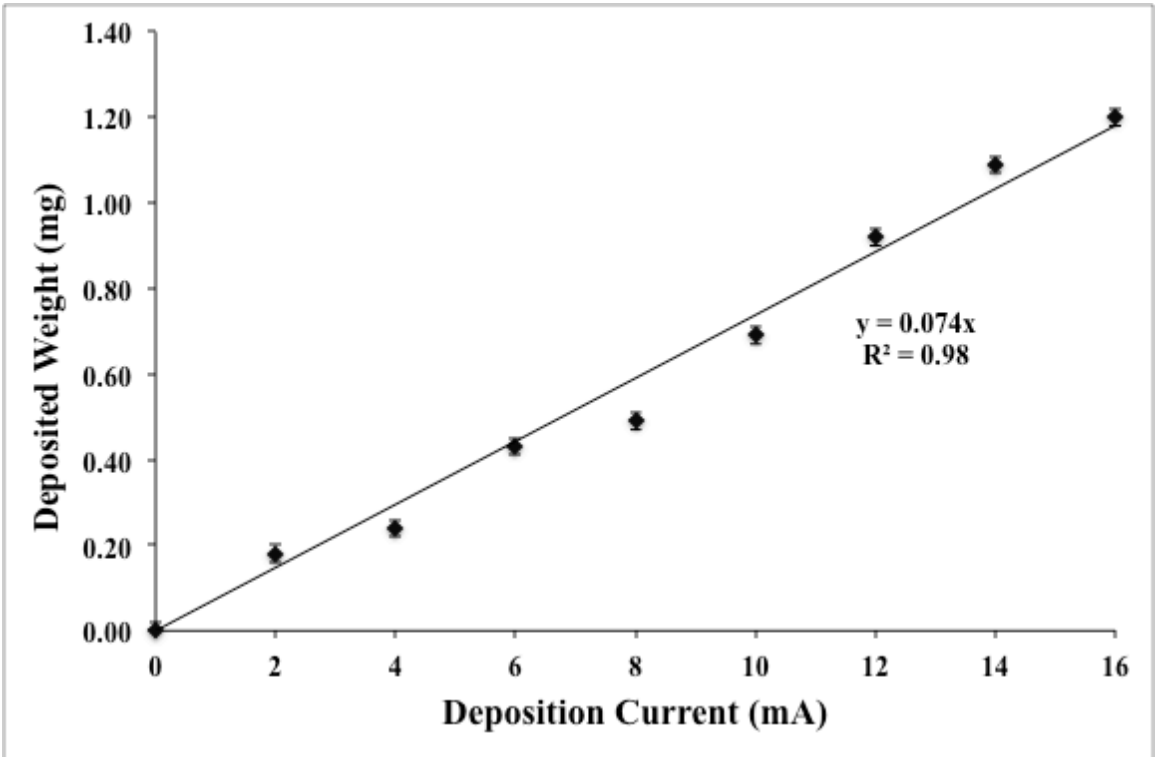

Figure 4.4: EPD deposit weight on aluminum (3.14 cm^2 deposition area) at a constant deposition time of 2 minutes for various deposition currents

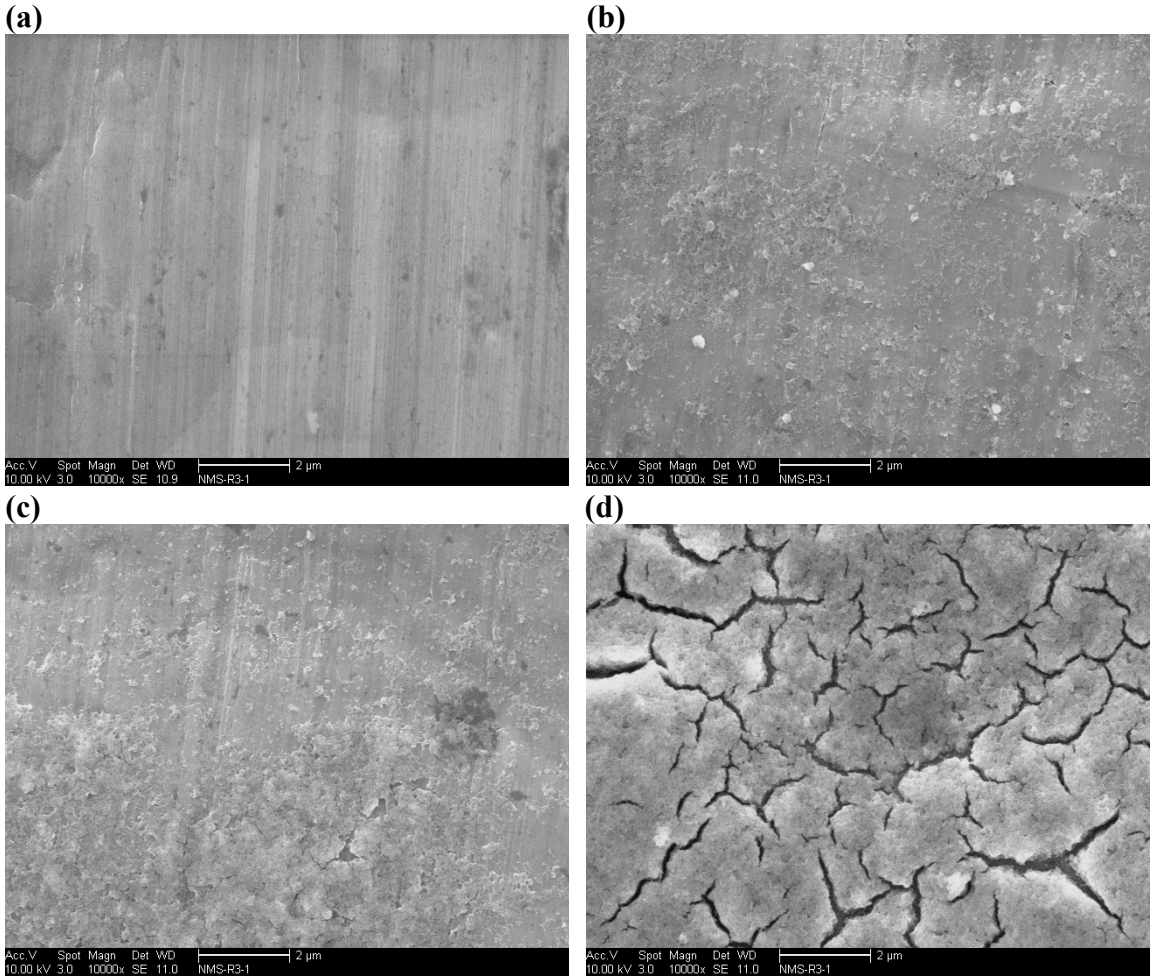

Figure 4.5: SEM micrographs of (a) blank aluminum substrate and EPD deposits at a constant time of 2 minutes, current of (b) 2 mA (c) 10 mA (d) 16 mA

4.3 EPD on Graphite Paper Substrates

4.3.1 Constant Deposition Time

Using the initial findings with EPD on aluminum substrates, the effects of EPD conditions on deposit morphologies on graphite paper substrates were investigated. Subsequently, the effects of morphology on the electrochemical activity of the EPD cobalt ferrite nanoparticle films were evaluated.

Electrophoretic deposition on graphite paper was first performed with a constant deposition current of 8 mA, while deposition time was varied between 30 seconds and 10 minutes. The deposited weight for each sample in this set is listed in Table 4.4. Similar to the deposits on aluminum substrates, when deposition current was held constant, deposited weight on the graphite paper increased with increasing deposition time, as expected. This relation is shown in Figure 4.6.

It was observed that as deposition time was increased, deposits for this set of samples gradually became thicker with a significant increase in deposit cracking. This progression is shown in Figure 4.7, where (a) has no cobalt ferrite deposited, (b) has regions of deposit and exposed substrate with slight deposit cracking, (c) has elevated deposit coverage, thickness, and deposit cracking compared to (b), and (d) has a relatively thick, uniform layer with significant deposit cracking.

The electrocatalytic activity of the EPD deposits on the graphite paper substrates was evaluated using linear sweep voltammetry. Figure 4.8 and Figure 4.9 show the variations in current density as a function of the applied voltage for samples deposited by EPD with varying deposition times. From this set of samples, Sample 103 (2 minutes deposition time, 0.20 mg deposit weight) showed the highest electrochemical activity

with a 2.84 mA/cm^2 increase in current density from the blank graphite paper, at an applied voltage of 0.9. In contrast, Sample 101 (30 seconds deposition time, 0.09 mg deposit weight) had the lowest activity with only a 1.01 mA/cm^2 increase in current density. Furthermore, Sample 103 tested 4.4 times greater than the blank graphite paper, while Sample 101 only tested 2.2 times greater than the blank control.

Taken together, the data in Figure 4.9, along with the corresponding SEM micrographs in Figure 4.7, suggest that a critical deposit thickness and degree of deposit cracking was achieved with Sample 103. Current density increased as the deposit weight increased from 0.09 to 0.20 mg as deposition time was increased from 30 seconds to 2 minutes. For deposition times greater than 2 minutes, with deposit weights larger than 0.20 mg, samples showed reduced electrocatalytic activity compared to the maximum observed with Sample 103, implying that thicker deposit layers and elevated deposit cracking may possibly hinder the electrocatalytic ability of deposits on graphite paper.

Table 4.4: Deposit weight and electrochemical data for EPD on graphite paper (3.14 cm^2 deposition area) at a deposition current of 8 mA for various deposition times

Sample Number	Deposition Time (min)	Deposited Weight (mg)	Current Density (mA/cm^2)*	i/i_{blank}
Blank	0.0	0.00	0.83	1.0
101	0.5	0.09	1.84	2.2
102	1.0	0.13	3.43	4.1
103	2.0	0.20	3.67	4.4
104	5.0	0.31	2.50	3.0
105	10.0	0.56	2.77	3.3

*Current density measurements taken at an applied voltage of 0.9

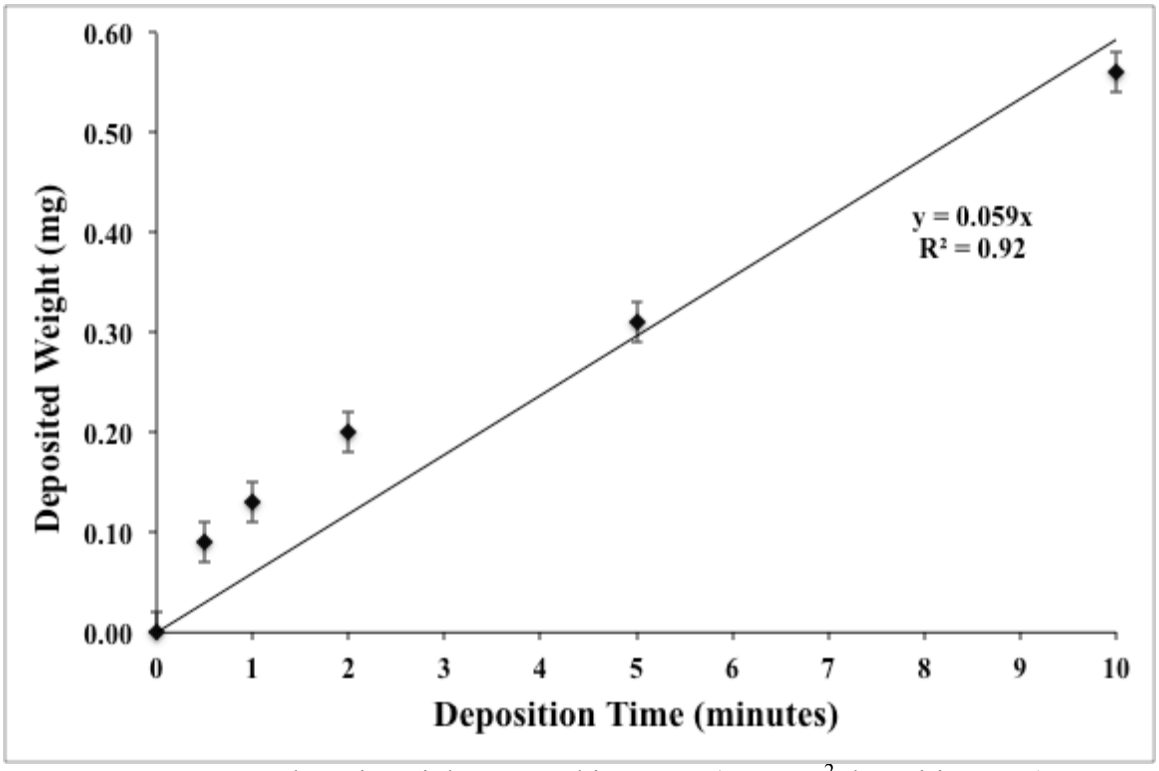

Figure 4.6: EPD deposit weight on graphite paper (3.14 cm^2 deposition area) at a constant deposition current of 8 mA for various deposition times

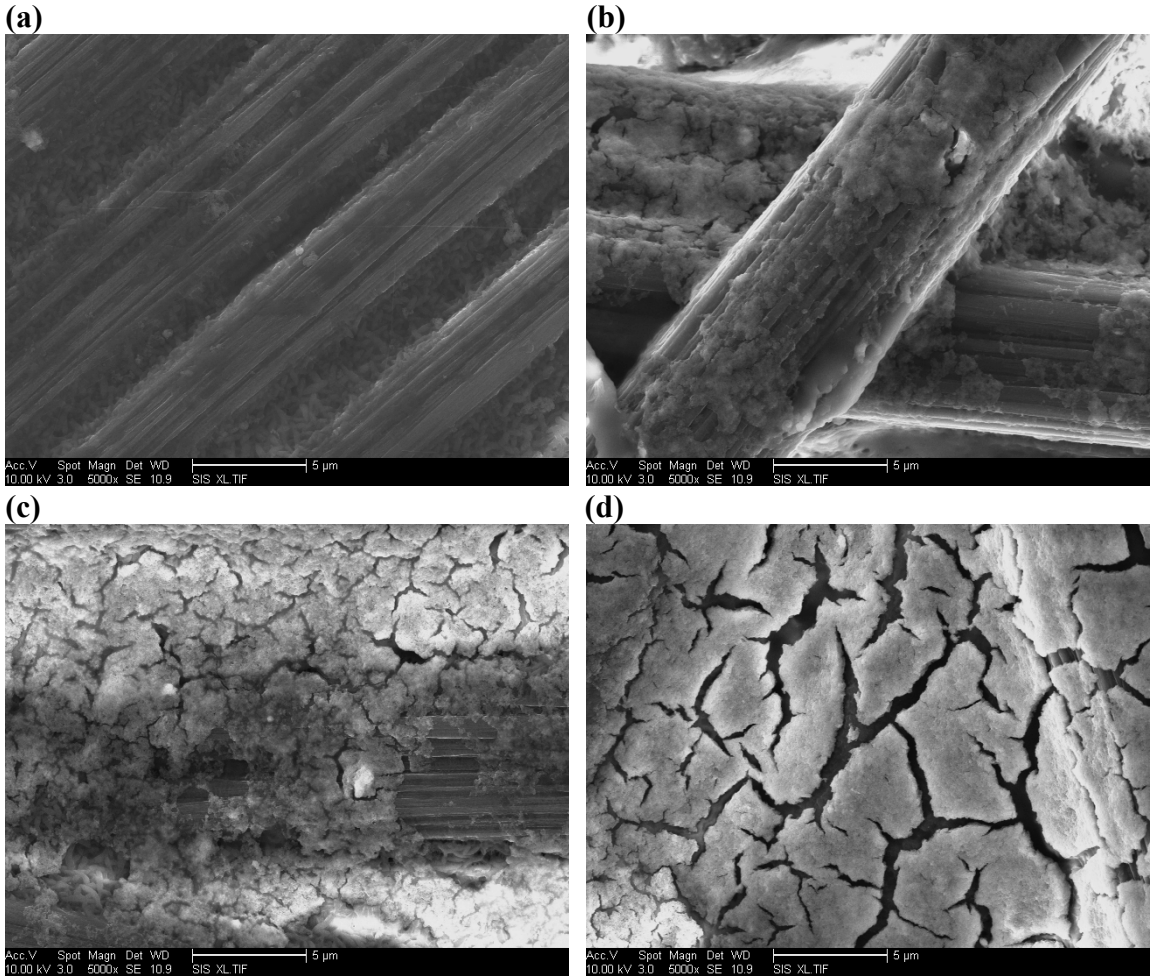

Figure 4.7: SEM micrographs of (a) blank graphite paper and EPD deposits at a constant current of 8 mA, time of (b) 30 seconds (c) 2 minutes (d) 10 minutes

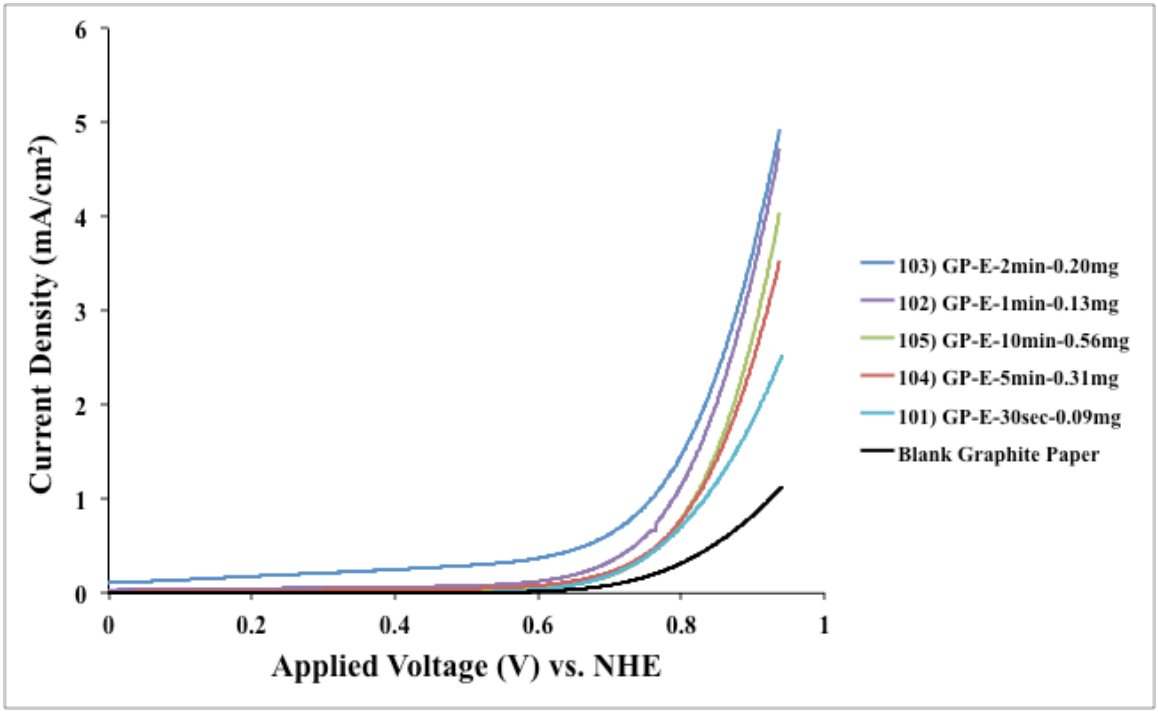

Figure 4.8: Electrocatalytic activity of EPD deposits (time varied, constant current) on graphite paper substrates in 2 M ammonium sulfite

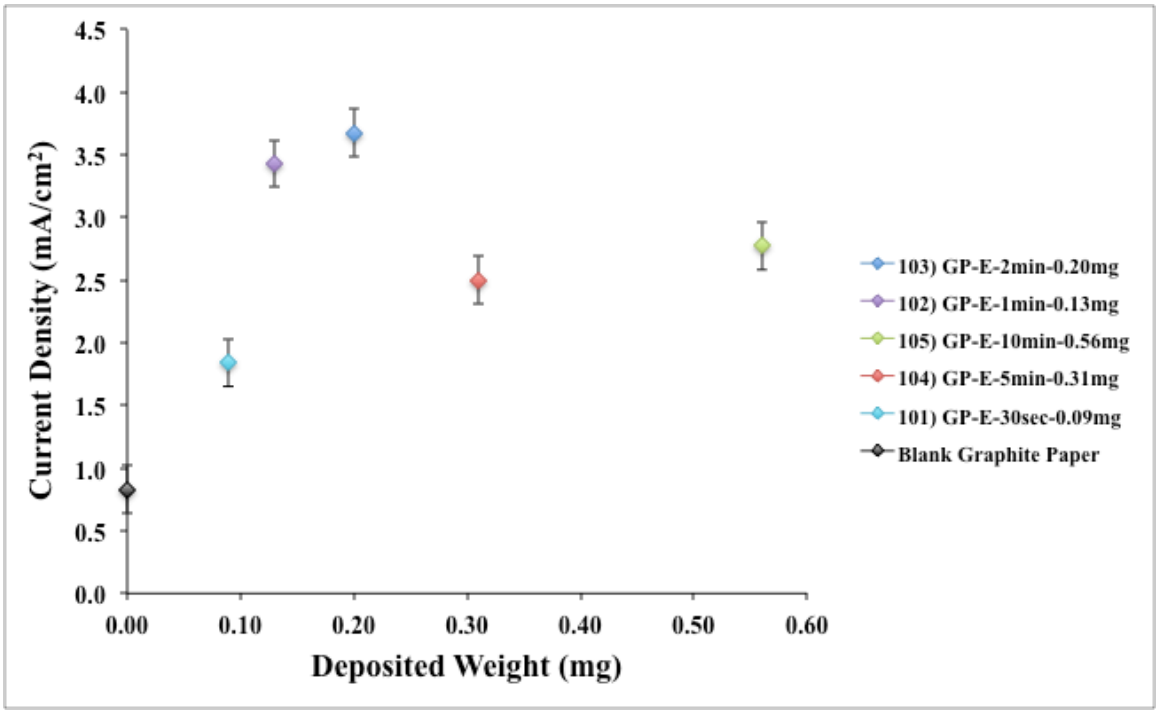

Figure 4.9: Current density of EPD deposits (time varied, constant current) on graphite paper substrates at 0.9 V (applied voltage vs. NHE)

4.3.2 Constant Deposition Current

In order to better understand why Sample 103 (2 minutes deposition time, 0.20 mg deposit weight) showed the highest electrochemical activity of the first set of EPD deposits on graphite paper (constant deposition current of 8 mA, varied deposition time) additional testing was performed to study the effects of deposition current on resulting deposits. Testing was conducted with a constant deposition time of 2 minutes while deposition current was varied from 0-16 mA in 2 mA increments (Table 4.5). The deposited weight for each corresponding deposition current is shown in Figure 4.10.

Figure 4.11 displays SEM micrographs of selected samples from this set. For the samples shown in Figure 4.11, (a) has no deposition, (b) has a uniformly thin, sparse deposition layer, (c) has deposit cracking and significantly less exposed graphite paper compared to (b), and (d) has a fully covered substrate, with cracking. It can readily be observed that as the mass of the deposit increased, with increasing deposition current, deposits became thicker and covered a larger portion of the graphite paper substrate. Additionally, deposit cracking became more prominent with increasing mass of the deposit.

Electrocatalytic activity of the samples varied significantly as deposition current was altered, as shown in Figures 4.12 and 4.13. Sample 106 (2 mA deposition current, 0.06 mg deposit weight) tested the lowest from this set of samples with a 0.44 mA/cm^2 increase in current density from the blank graphite paper at an applied voltage of 0.9 V. As a result of small amount of deposited weight on Sample 106, substantial portions of the graphite paper substrate remained exposed (Figure 4.11b). The largest increase in electrocatalytic activity on graphite paper was observed with Sample 110 (10 mA

deposition current, 0.29 mg deposit weight). The increase in current density from blank graphite paper was measured to be 3.77 mA/cm^2 (5.5x better than the blank). The deposit layer for Sample 110 covered most of the graphite paper surface and was thick enough to introduce cracking, as shown in Figure 4.11c.

Similar to the varied deposition time data, the data in Figure 4.13 implies that a critical deposit thickness, coverage, and degree of cracking is achieved with Sample 110, resulting in the highest current density amongst all graphite paper samples. For samples that had a larger deposited weight than Sample 110, deposition current greater than 10 mA, electrochemical activity decreased.

To estimate the critical deposit thickness achieved with Sample 110, calculations were performed to find the number of particle layers present, assuming hexagonal close packing. The mass of a monolayer per cm^2 of the 20 nm cobalt ferrite nanoparticles was determined to be 10.2 μg/cm^2 [1]. Additionally, the surface area and areal density of the graphite paper was specified to be 0.07 m^2/g and 34 g/m^2 (Figure A.2), respectively [1]. For the substrate area of 3.14 cm^2 on graphite paper, the deposit weight for a monolayer was calculated to be 0.076 mg [1]. Sample 110 had a deposit weight of 0.29 mg; thus, if the deposit was completely uniform and fully covered the graphite paper surface, there would be approximately 3.1 layers present. Based on the electrochemical data, and the validity of the stated assumptions, the most electrochemically active deposit thickness on graphite paper for 20 nm cobalt ferrite nanoparticles would be roughly 3.1 layers. The cracking observed in Figure 4.11c suggests that multiple layers of the nanoparticles are present in Sample 110, agreeing with the number of estimated particle layers.

Figure 4.14 draws a comparison between Sample 110 (10 mA deposition current, 0.29 mg deposit weight) and a platinum cobalt deposition under the same conditions. The platinum cobalt sample exceeded the performance of the blank graphite paper substrate by a factor of nearly 10. The current density of Sample 110 was roughly 56% of its platinum cobalt comparison, at an applied voltage of 0.9.

Table 4.5: Deposit weight and electrochemical data for EPD on graphite paper (3.14 cm^2 deposition area) at a deposition time of 2 minutes for various deposition currents

Sample Number	Deposition Current (mA)	Deposited Weight (mg)	Current Density (mA/cm^2)*	i/i_{blank}	i/i_{Pt}
Blank	0	0.00	0.83	1.0	0.10
106	2	0.06	1.27	1.5	0.15
107	4	0.10	1.84	2.2	0.22
108	6	0.18	1.90	2.3	0.23
109	8	0.23	3.54	4.3	0.43
110	10	0.29	4.60	5.5	0.56
111	12	0.37	3.67	4.4	0.45
112	14	0.40	3.87	4.7	0.47
113	16	0.47	2.34	2.8	0.28
Pt_3Co	10	0.59	8.25	9.9	1.00

*Current density measurements taken at an applied voltage of 0.9

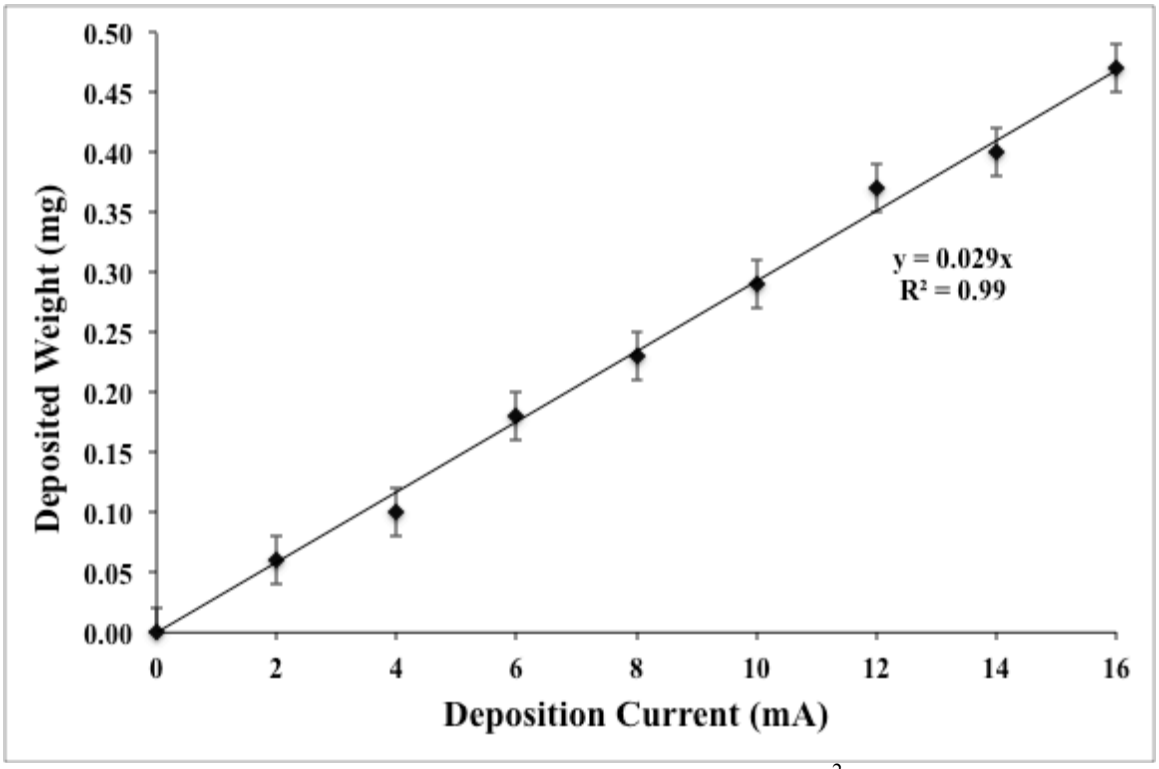

Figure 4.10: EPD deposit weight on graphite paper (3.14 cm^2 deposition area) at a constant deposition time of 2 minutes for various deposition currents

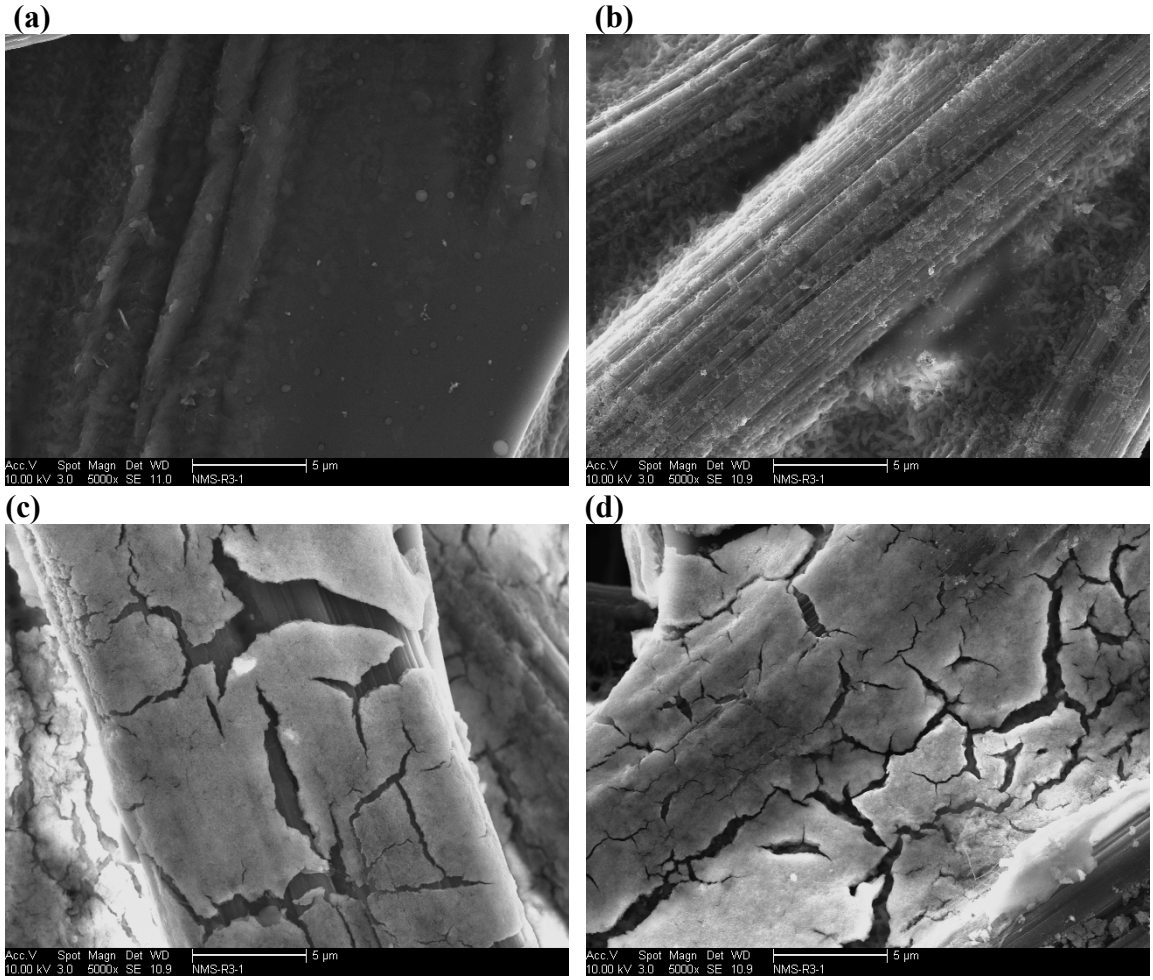

Figure 4.11: SEM micrographs of (a) blank graphite paper and EPD deposits at a constant time of 2 minutes, current of (b) 2 mA (c) 10 mA (d) 16 mA

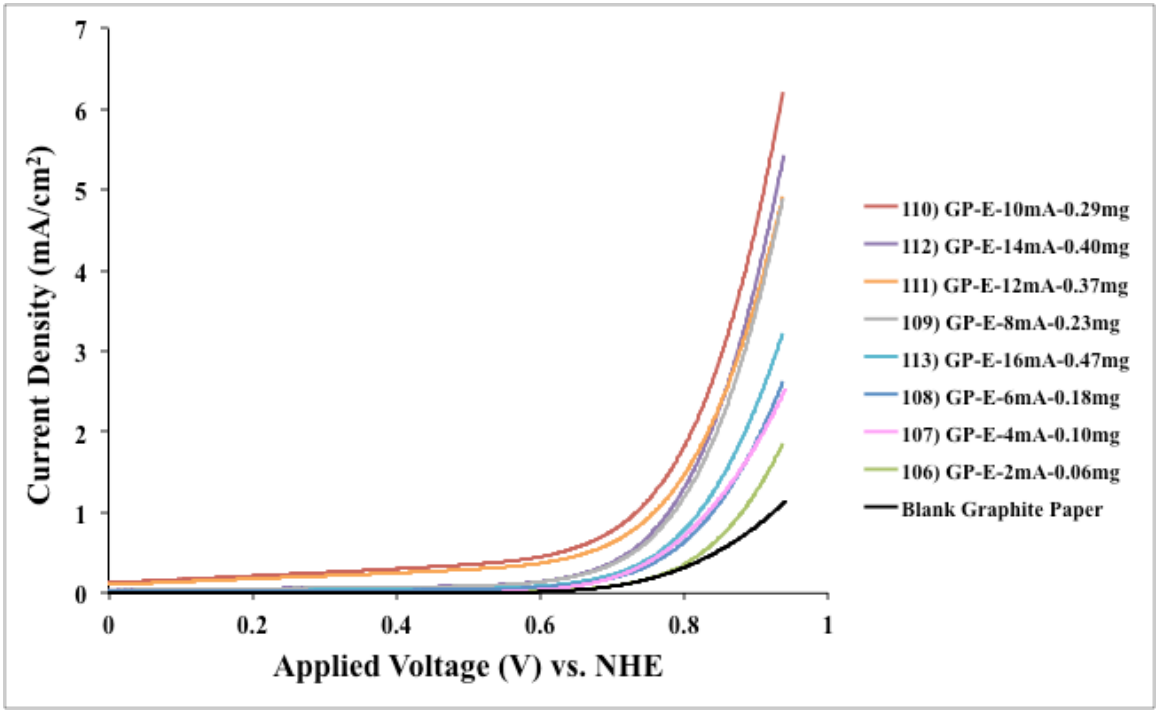

Figure 4.12: Electrocatalytic activity of EPD deposits (current varied, constant time) on graphite paper substrates in 2 M ammonium sulfite

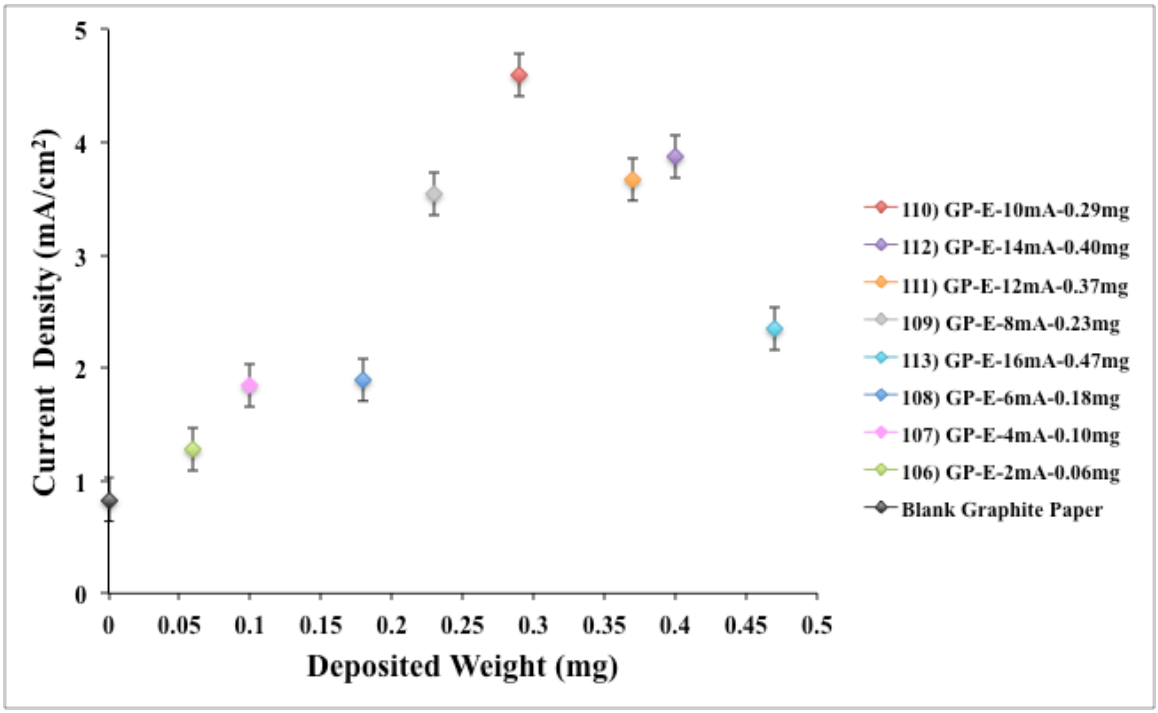

Figure 4.13: Current density of EPD deposits (current varied, constant time) on graphite paper substrates at 0.9 V (applied voltage vs. NHE)

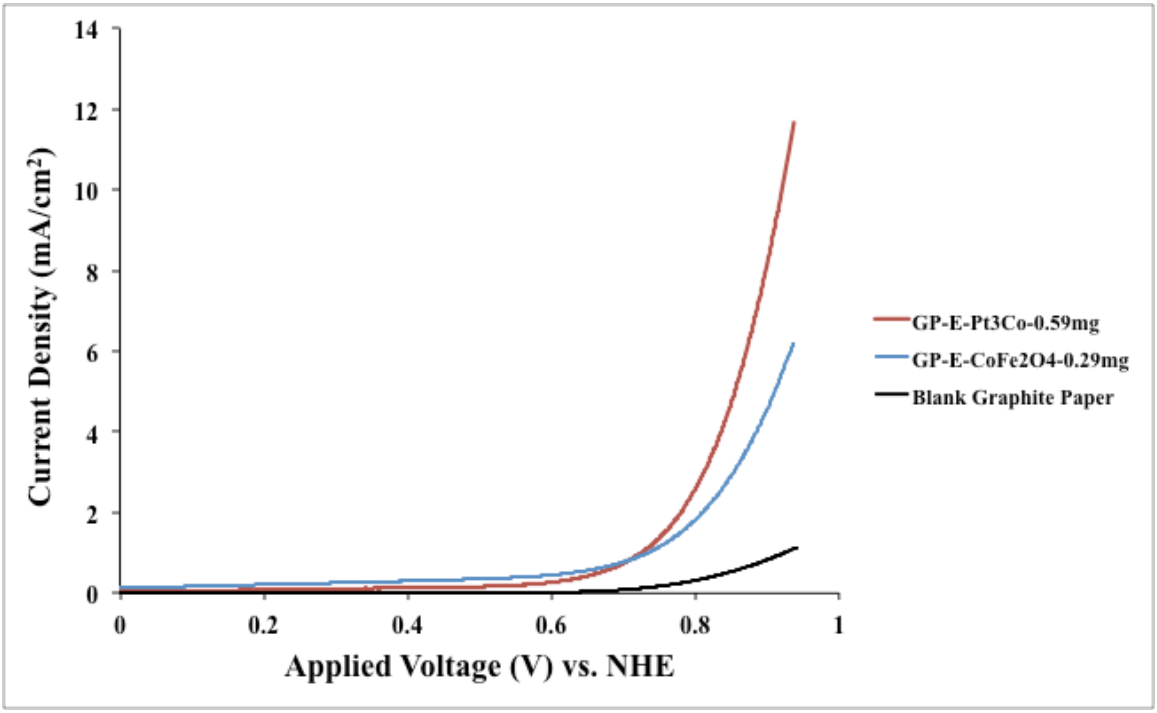

Figure 4.14: Comparison of electrocatalytic activity between cobalt ferrite and platinum cobalt samples at the same EPD conditions of 10 mA and 2 minutes on graphite paper in 2 M ammonium sulfite

4.4 EPD on Carbon Felt Substrates

4.4.1 Constant Deposition Time

EPD of nanoparticles on 3D carbon felt substrates (3 mm thickness) was compared to graphite paper. Analogous to the aluminum and graphite paper tests, EPD was first performed with a constant current of 8 mA, while deposition time was varied from 30 seconds to 10 minutes. The deposited weight on each sample and its corresponding deposition time is listed in Table 4.6. As observed with the prior substrates, deposited weight increased with longer EPD deposition times (Figure 4.15).

Figure 4.16 presents SEM micrographs of select samples from this experiment set, where (a) had no cobalt ferrite deposited, (b) had a thin, uniform coating of deposit, (c) had a non-uniform increase in deposit thickness relative to (b), and (d) had a thick enough layer to introduce cracks in the deposit. As deposition time was increased, deposits began to lose uniformity due to the cobalt ferrite depositing multiple layers on different regions of the substrate.

In accordance with tests on graphite paper samples, deviations in deposit morphologies greatly impacted corresponding electrocatalytic activity. The extent of these variations is shown in Figure 4.17 and Figure 4.18. Sample 201 (30 seconds deposition time, 0.21 mg deposit weight) tested the highest for varied deposition time samples with an elevated current density of 66.7 mA/cm^2 from the blank carbon felt, at an applied voltage of 0.9. Conversely, Sample 202 (1 minute deposition time, 0.25 mg deposit weight) tested the lowest with a 47.8 mA/cm^2 increase in current density from the blank carbon felt.

Comparing the electrochemical test data presented in Figure 4.18 with the corresponding SEM micrographs in Figure 4.16 suggests that a critical deposit thickness was achieved with Sample 201 (30 seconds deposition time, 0.21 mg deposit weight). Current density immediately peaked at a deposition time of 30 seconds and then dropped to a minimum for a 1 minute deposition time (Figure 4.18). Increased deposition time beyond 1 minute for the varied deposition time samples resulted in minimal changes in electrocatalytic activity. This trend is analogous to the results found on graphite paper samples, further supporting the hypothesis that a deposit thickness threshold exists where at a certain point, depositing more cobalt ferrite particles diminishes electrocatalytic activity. For varied deposition time samples on carbon felt, electrocatalytic activity peaked at the 30 seconds, whereas for graphite paper, the apex occurred at 2 minutes.

Further EPD was performed on carbon felt holding deposition time constant, while varying deposition current.

Table 4.6: Deposit weight and electrochemical data for EPD on carbon felt (2 cm^2 deposition area) at a deposition current of 8 mA for various deposition times

Sample Number	Deposition Time (min)	Deposited Weight (mg)	Current Density (mA/cm^2)*	i/i_{blank}
Blank	0.0	0.00	20.3	1.0
201	0.5	0.21	87.0	4.3
202	1.0	0.25	68.1	3.4
203	2.0	0.34	72.4	3.6
204	5.0	0.54	70.1	3.5
205	10.0	0.71	77.5	3.8

*Current density measurements taken at an applied voltage of 0.9

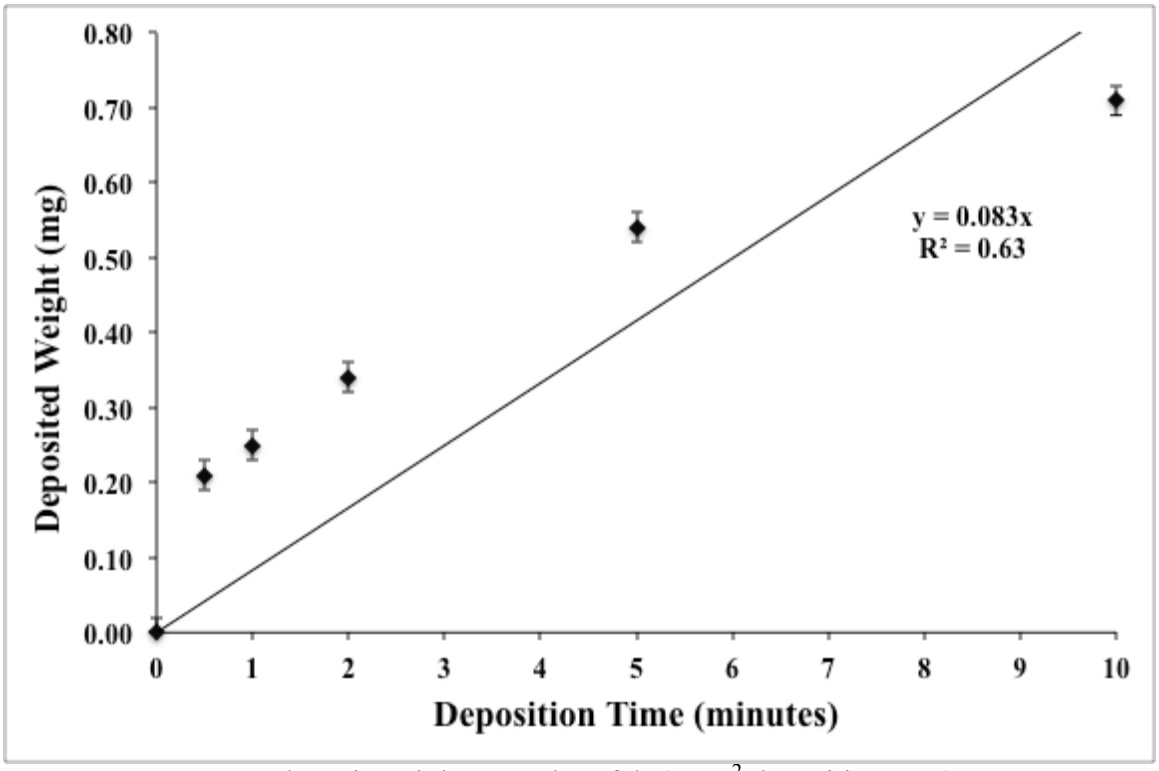

Figure 4.15: EPD deposit weight on carbon felt (2 cm^2 deposition area) at a constant deposition current of 8 mA for various deposition times

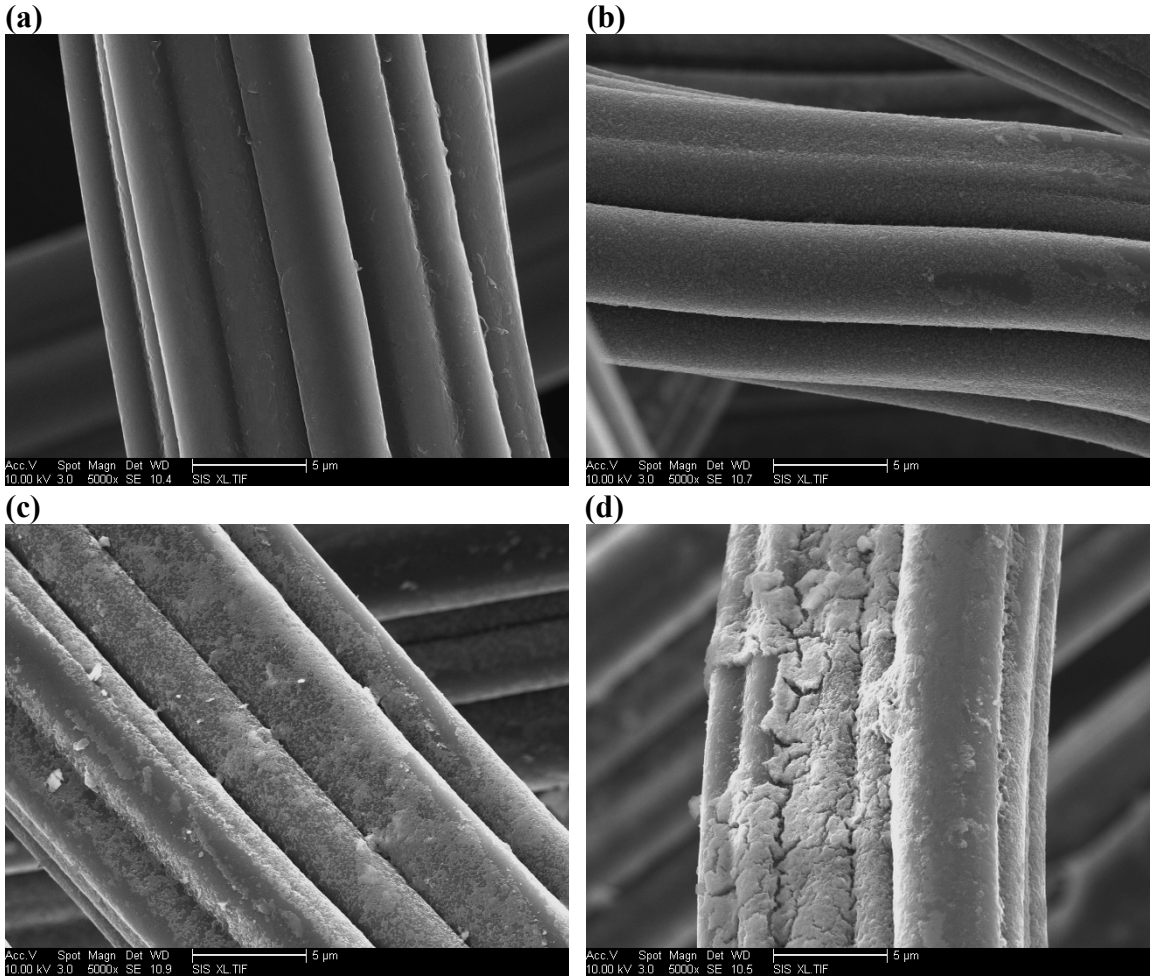

Figure 4.16: SEM micrographs of (a) blank carbon felt and EPD deposits at a constant current of 8 mA, time of (b) 30 seconds (c) 1 minute (d) 5 minutes

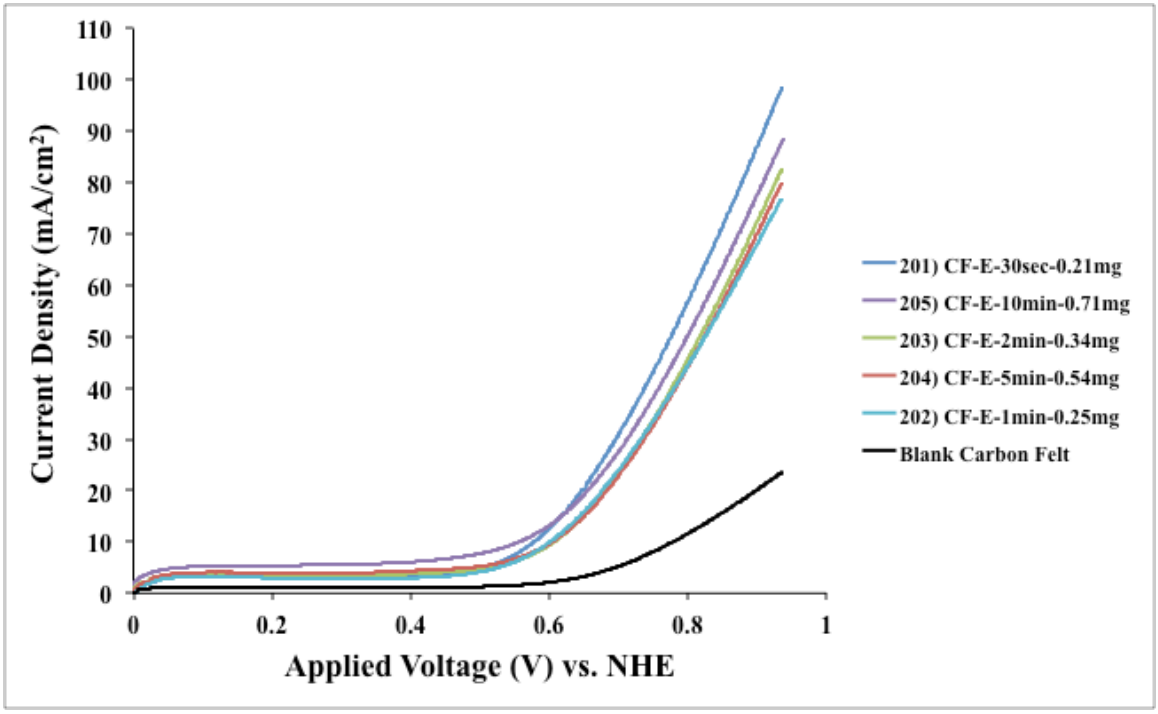

Figure 4.17: Electrocatalytic activity of EPD deposits (time varied, constant current) on carbon felt substrates in 2 M ammonium sulfite

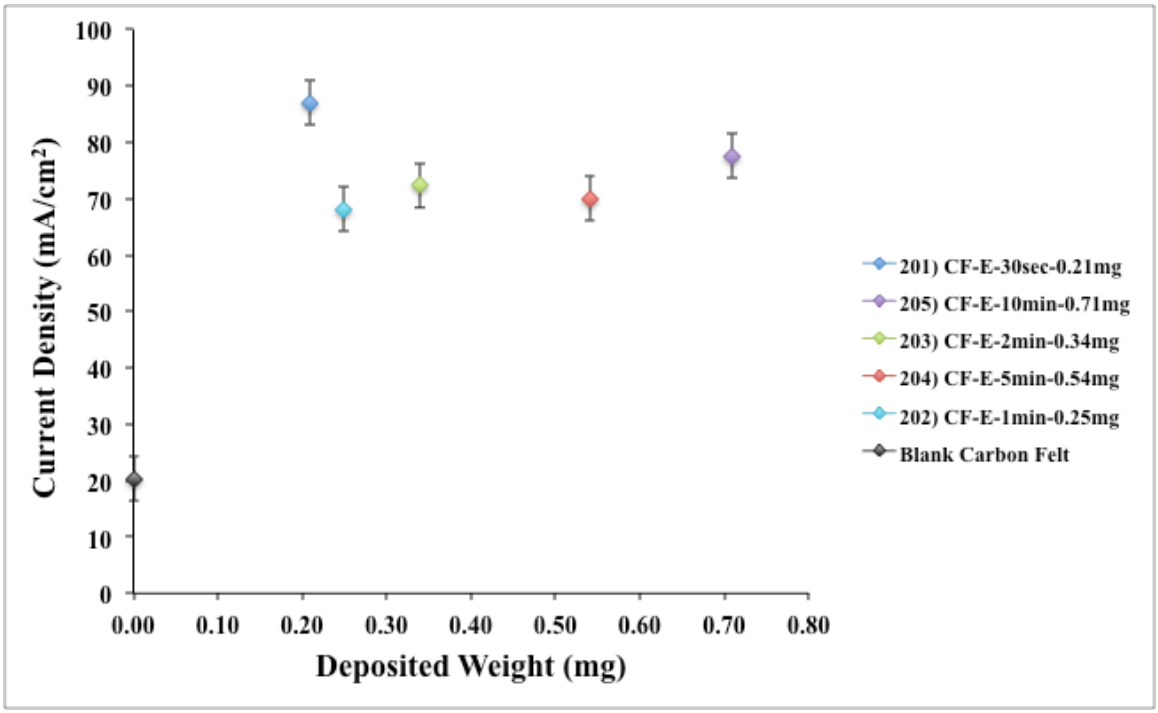

Figure 4.18: Current density of EPD deposits (time varied, constant current) on carbon felt substrates at 0.9 V (applied voltage vs. NHE)

4.4.2 Constant Deposition Current

To explore the influence of EPD deposition current on the deposit morphology for carbon felt substrates, deposition time was held at a constant 30 seconds for each sample, while deposition current was varied from 0-16 mA in 2 mA increments (Table 4.7). The relation between deposit weight and deposition current was nearly linear for the carbon felt samples, as shown in Figure 4.19. The increase in deposit weight can be observed in Figure 4.20, where (a) has no cobalt ferrite deposited, (b) has an extremely sparse, thin deposit, (c) has a thin, uniform deposit with significantly less exposed substrate than (b), and (d) has a completely covered, thicker deposit. As deposition current was increased, both deposit coverage and thickness proportionally increased. Additionally, deposit uniformity was preserved with increasing deposition current, dissimilar from the varied deposition time experiments performed on carbon felt.

As observed with prior tests, changes in deposit morphology, led to substantial changes in electrocatalytic activity as shown in Figures 4.21-4.22. Sample 209 (8 mA deposition current, 0.23 mg deposit weight) had the highest activity with an increased current density of 67.1 mA/cm^2 from the blank carbon felt, at an applied voltage of 0.9. In contrast, Sample 206 (2 mA deposition current, 0.11 deposit weight) had the lowest activity with a 38.9 mA/cm^2 improvement from the blank carbon felt.

Combining the electrochemical test results for varied deposition current samples with the SEM micrographs presented in Figure 4.20 further supports the notion that a critical deposit thickness exists at which electrocatalytic activity peaks. This point was attained by Sample 209 for the constant deposition current carbon felt experiments. Current density progressively increased with each increment in deposition current until

the maximum observed at 8 mA (Sample 210). As EPD deposition current was raised past this point, the current density of the resulting deposit began to decline and appeared to level off at approximately 65 mA/cm^2, a 45 mA/cm^2 increase from the blank carbon felt.

To estimate the critical deposit thickness achieved with Sample 209, calculations were performed in a similar manner to the aluminum and graphite paper substrates to determine the number of particle layers present. The mass of a monolayer per cm^2 of the 20 nm cobalt ferrite nanoparticles was determined to be 10.2 μg/cm^2 [1]. Furthermore, the surface area and areal density of the carbon felt was specified to be 0.6 m^2/g and 280 g/m^2, respectively (Figure A.3). For the substrate area of 1 cm^2 on carbon felt, the deposit weight for a monolayer was calculated to be 1.71 mg. Sample 209 had a deposit weight of 0.23 mg; thus, if the deposit for Sample 209 was uniform and completely covered the exposed surface of the carbon felt, there would be approximately 0.13 layers present. The SEM micrograph of the outer surface of Sample 209 displayed in Figure 4.20c appears to have a thin, well-covered deposit. Comparing the layer calculation to the corresponding SEM image suggests that there were regions on Sample 209 that were not fully coated with the cobalt ferrite nanoparticles and that the deposit was not completely uniform throughout the entire sample. After splicing the substrate, further SEM analysis was performed at the middle of Sample 209 to investigate the overall deposit uniformity throughout the sample (Figure 4.23). It is readily observed that particles did not completely penetrate the carbon felt, as the deposit at the middle of the sample has several regions of exposed substrate. Further analysis regarding the penetration of cobalt ferrite into 3D substrates was completed by Nicole Pacheco [1].

Figure 4.24 shows a comparison between Sample 209 (8 mA deposition current, 0.23 mg deposit weight) and a platinum cobalt deposition under the same conditions. The platinum cobalt sample exceeded the performance of the blank graphite paper substrate nearly seven-fold. The current density of Sample 209 was roughly 58% of its platinum cobalt comparison, at an applied voltage of 0.9.

Table 4.7: Deposit weight and electrochemical data for EPD on carbon felt (2 cm^2 deposition area) at a deposition time of 30 seconds for various deposition currents

Sample Number	Deposition Current (mA)	Deposited Weight (mg)	Current Density (mA/cm^2)*	i/i_{blank}	i/i_{Pt}
Blank	0	0.00	20.3	1.0	0.13
206	2	0.11	58.9	2.9	0.39
207	4	0.14	62.8	3.1	0.42
208	6	0.18	76.4	3.8	0.51
209	8	0.23	87.6	4.3	0.58
210	10	0.28	74.3	3.7	0.49
211	12	0.33	63.5	3.1	0.42
212	14	0.37	65.9	3.3	0.44
213	16	0.45	66.4	3.3	0.44
Pt_3Co	8	0.89	151.2	7.4	1.00

*Current density measurements taken at an applied voltage of 0.9

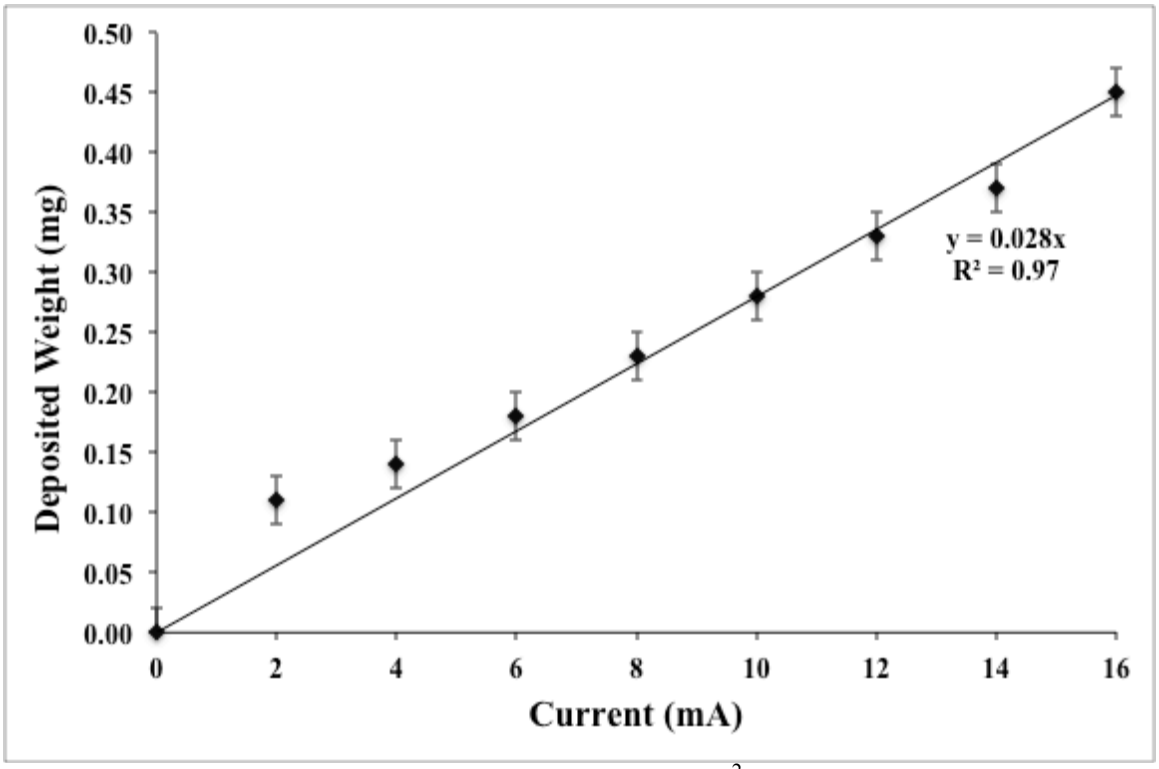

Figure 4.19: EPD deposit weight on carbon felt (2 cm^2 deposition area) at a constant deposition time of 30 seconds for various deposition currents

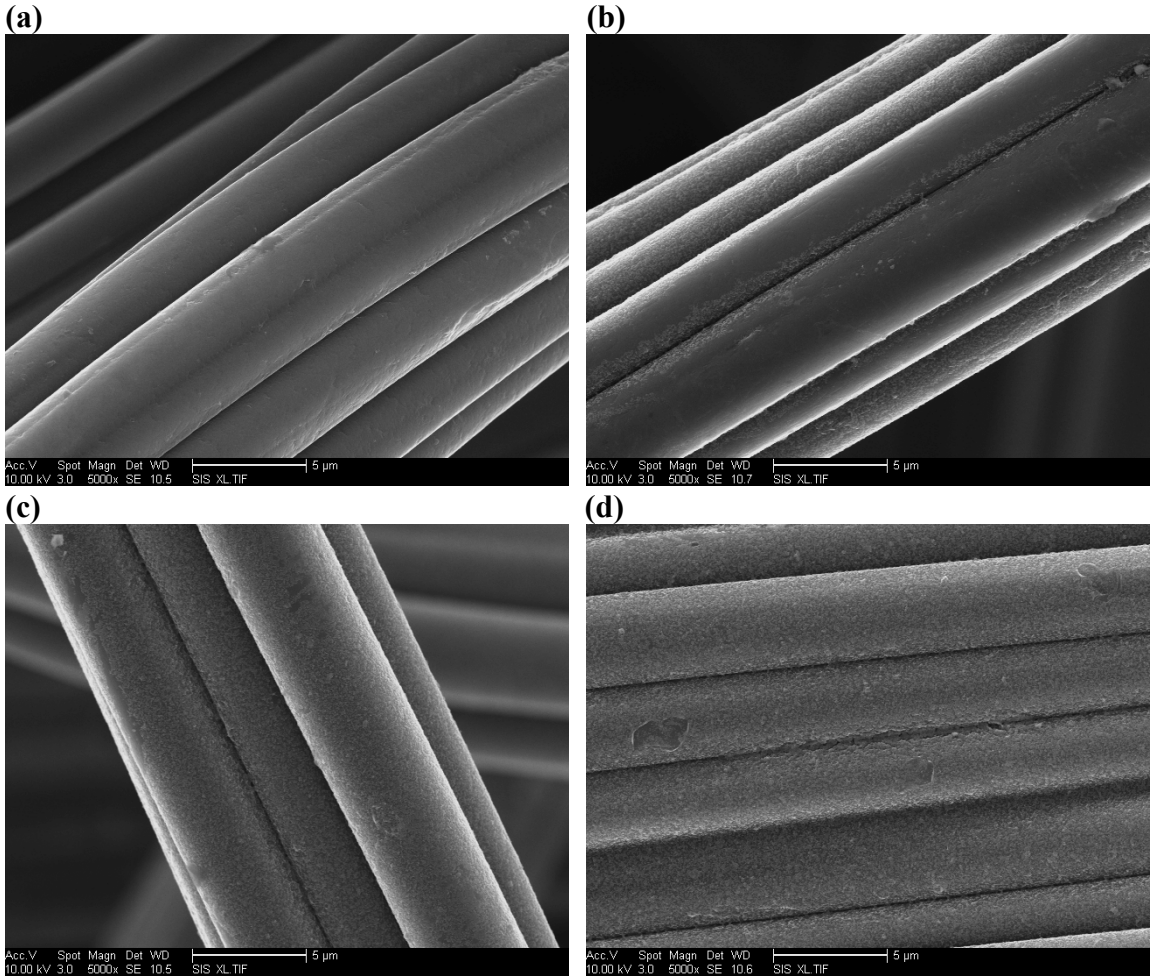

Figure 4.20: SEM micrographs of (a) blank carbon felt and EPD deposits at a constant time of 30 seconds, current of (b) 2 mA (c) 8 mA (d) 16 mA

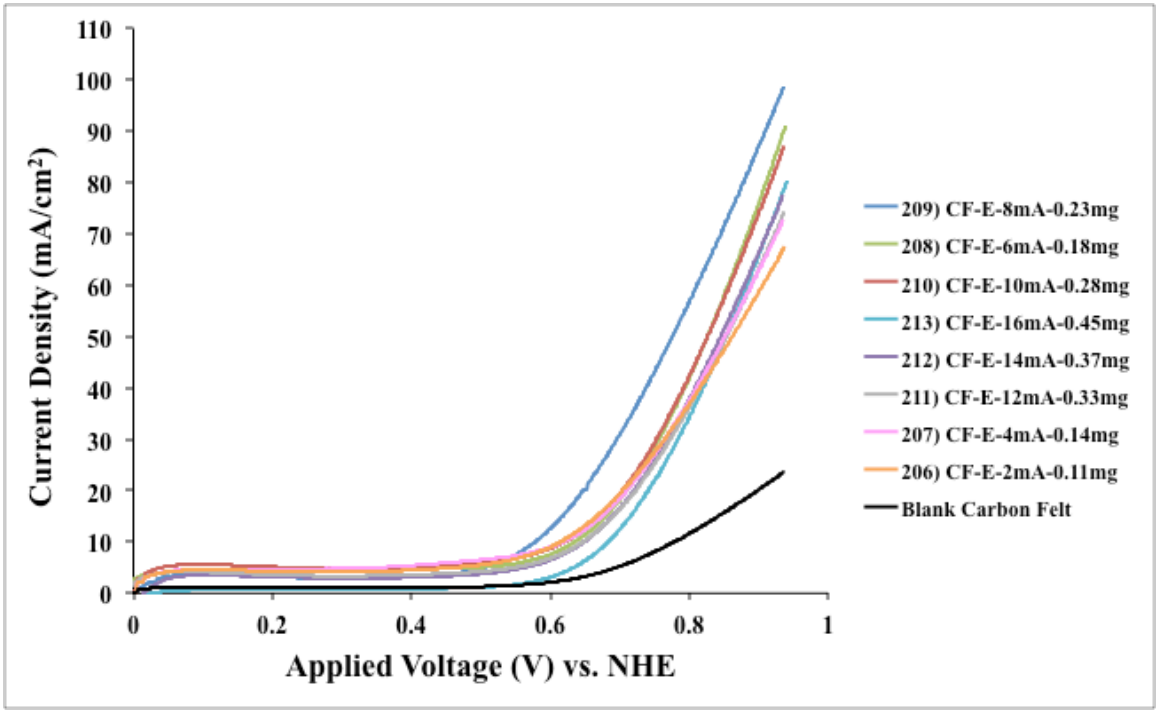

Figure 4.21: Electrocatalytic activity of EPD deposits (current varied, constant time) on carbon felt substrates in 2 M ammonium sulfite

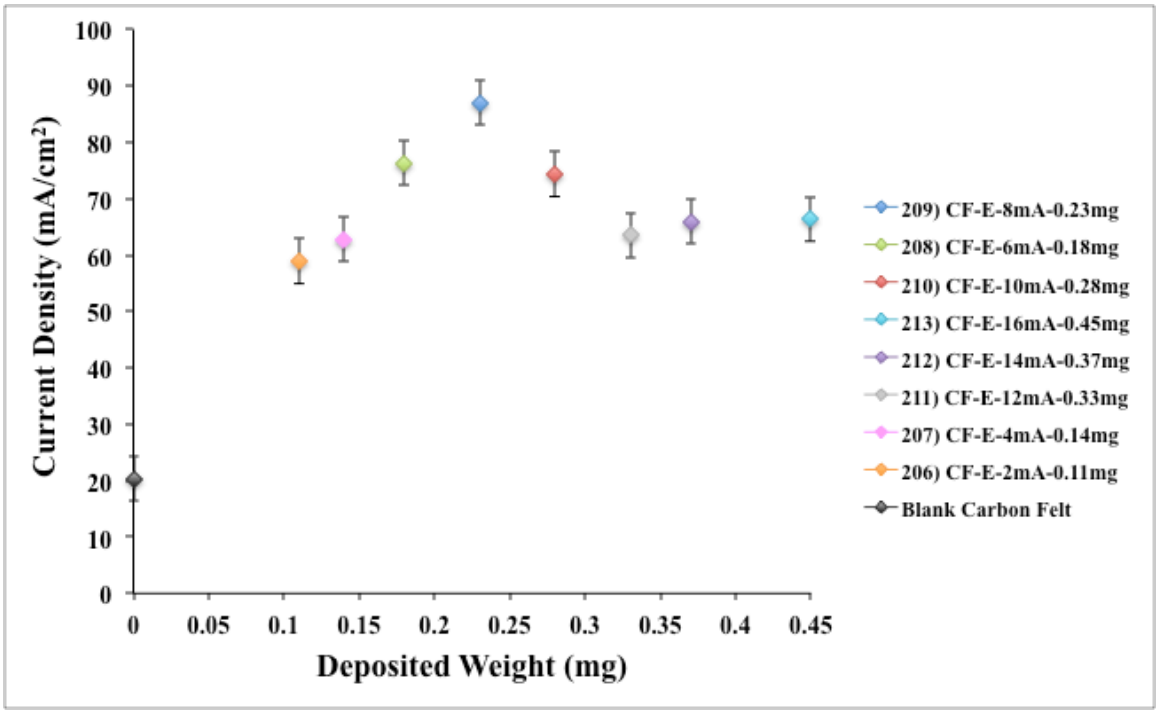

Figure 4.22: Current density of EPD deposits (current varied, constant time) on carbon felt substrates at 0.9 V (applied voltage vs. NHE)

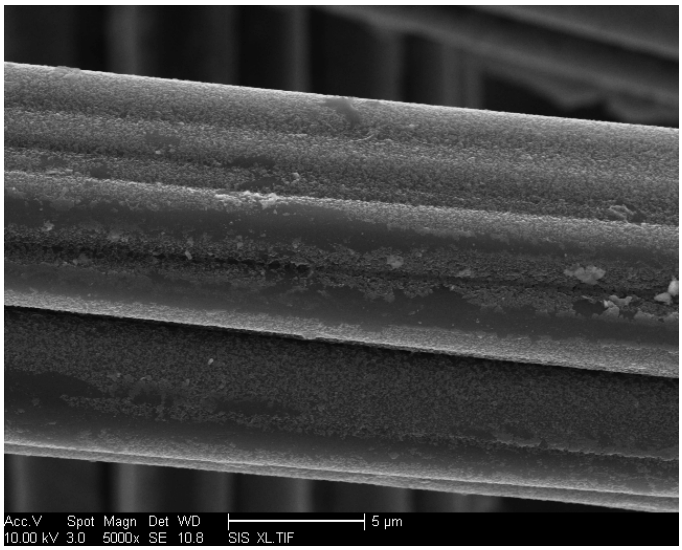

Figure 4.23: SEM micrograph of spliced EPD deposit at a deposition time of 30 seconds, current of 8 mA on carbon felt (middle of sample)

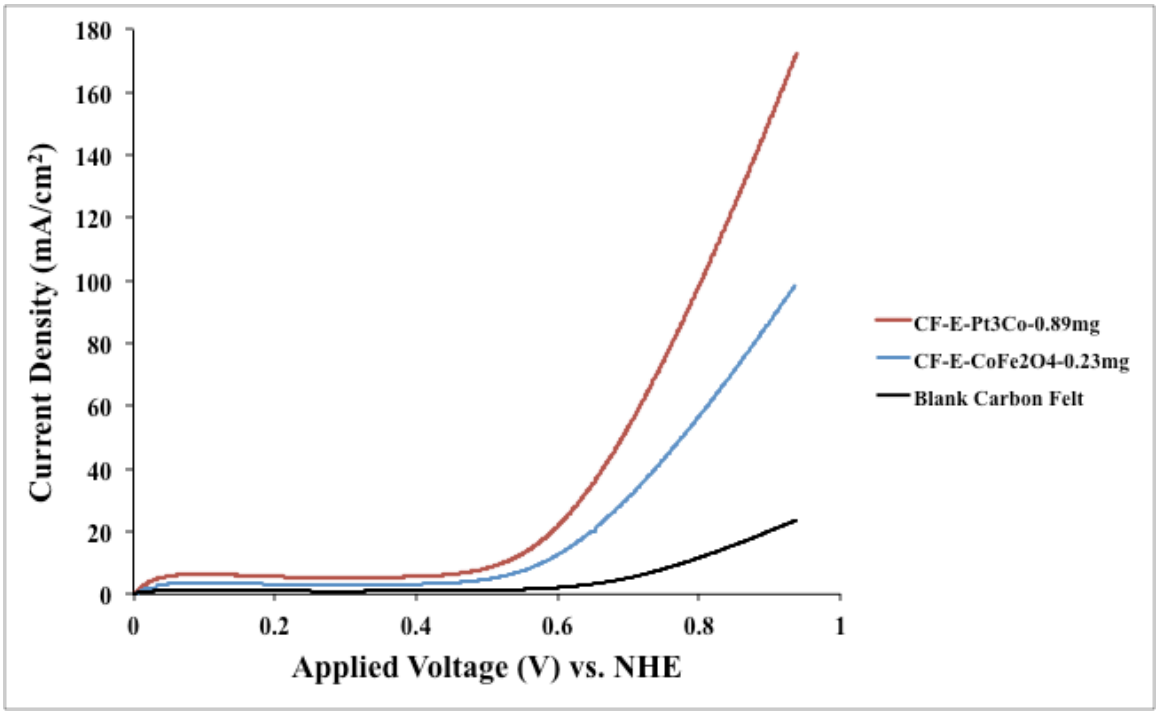

Figure 4.24: Comparison of electrocatalytic activity between cobalt ferrite and platinum cobalt samples at the same EPD conditions of 8 mA and 30 seconds on carbon felt in 2 M ammonium sulfite

4.5 Comparison of EPD on Various Substrates

Comparisons were drawn between the EPD deposits on aluminum, graphite paper and carbon felt. The rate of deposition for constant deposition current (8 mA), varied deposition time EPD on each substrate and corresponding deposit weight range are listed in Table 4.8. EPD performed on aluminum resulted in the greatest deposition rate of cobalt ferrite nanoparticles, approximately 1.8 and 1.3 times more than on graphite paper and carbon felt, respectively. Furthermore, dip-tests for all substrates resulted in no deposited particles.

Information regarding deposit weight and particle layer ranges for EPD on the different substrates is shown in Table 4.10. EPD on all substrates generally followed the same trend in regards to deposit morphology. As deposit weight was increased due to increasing deposition current or time, deposit sparsity diminished and eventually deposits became thick enough to introduce cracking. Every sample set exhibited some degree of cracking at larger deposit weights, except for EPD at constant deposition time, varied deposition current on carbon felt. From this EPD set, the largest deposit weight was for Sample 213 (16 mA deposition current, 0.45 mg deposit weight). An SEM micrograph of Sample 213 is shown in Figure 4.20d, where no cracking is observed.

Table 4.11 lists the largest current densities measured and the corresponding particle layer estimation for both graphite paper and carbon felt. The most electrochemically active sample on graphite paper (Sample 110) had a current density of 4.60 mA/cm^2, which was 5.5 times greater than the blank graphite paper. Furthermore, its current density was roughly 56% of the platinum cobalt comparison, under the same EPD conditions. It was estimated that Sample 110 had about 3 nanoparticle layers. For

carbon felt, Sample 209 was found to be the most electrochemically active sample with a current density of 87.6 mA/cm^2. Sample 209 tested 4.3 times better than the blank carbon felt substrate. Moreover, its current density was roughly 58% of its platinum cobalt comparison, under the same EPD conditions. It was estimated that Sample 209 had approximately 0.1 of a particle layer.

Table 4.8: Rate of deposition for EPD on various substrates at a constant deposition current of 8 mA and deposit weight range (includes dip-tests)

Substrate	Deposit Weight Range (mg)	Slope (mg/minute)
Aluminum	0 − 0.92	0.107
Graphite Paper	0 − 0.56	0.059
Carbon Felt	0 − 0.71	0.083

Table 4.9: Geometric area, surface area, and areal density information for graphite paper and 3 mm carbon felt substrates

Substrate	Geometric Area (cm^2)	Surface Area (m^2/g)	Areal Density (g/m^2)
Graphite Paper	3.14	0.07	34
Carbon Felt	1	0.6	280

Table 4.10: EPD deposit weight range for different substrates and corresponding estimated particle layer range

Substrate	Deposit Weight Range (mg)	Number of Particle Layers Range
Aluminum	0.18 − 1.20	5 − 30
Graphite Paper	0.06 − 0.56	0.8 − 6
Carbon Felt	0.11 − 0.71	0.06 − 0.4

Table 4.11: Largest current densities obtained for EPD on graphite paper and carbon felt and corresponding estimated number of particle layers

Substrate	Current Density (mA/cm^2)*	i/i_{blank}	i/i_{Pt}	Number of Particle Layers
Graphite Paper	4.60	5.5	0.56	3
Carbon Felt	87.6	4.3	0.58	0.1

*Current density measurements taken at an applied voltage of 0.9

4.6 Reproducibility

Experiments to check the reproducibility of the results were performed for EPD on both graphite paper and carbon felt substrates. The EPD conditions for these tests were selected based on the most electrochemically active samples for the graphite paper and carbon felt experiments, respectively.

For the graphite paper samples, the deposition current was 10 mA and deposition time was 2 minutes. The resulting deposit weights and current densities are listed in Table 4.12. Figure 4.25 presents the corresponding LSV graph. The standard deviation in deposit weight for the five EPD deposits on graphite paper was determined to be 0.02 mg, while the standard deviation in current density at an applied voltage of 0.9 V was found to be 0.2 mA/cm^2.

For the EPD deposits on carbon felt substrates, the deposition current was 8 mA and deposition time was 30 seconds. The resulting deposit weights and current densities are listed in Table 4.13. Figure 4.26 shows the associated LSV graph. The standard deviation in deposit weight for the five EPD deposits on carbon felt was determined to be 0.02 mg, while the standard deviation in current density at an applied voltage of 9.0 V was determined to be 4.0 mA/cm^2.

Table 4.12: Deposit weight and electrochemical data for EPD on graphite paper (3.14 cm^2 deposition area) at a deposition current of 10 mA and deposition time of 2 minutes

Sample Number	Deposited Weight (mg)	Current Density (mA/cm^2)*
Blank	0.00	0.83
114	0.20	3.98
115	0.21	3.55
116	0.24	3.70
117	0.23	3.41
118	0.25	3.77

*Current density measurements taken at an applied voltage of 0.9

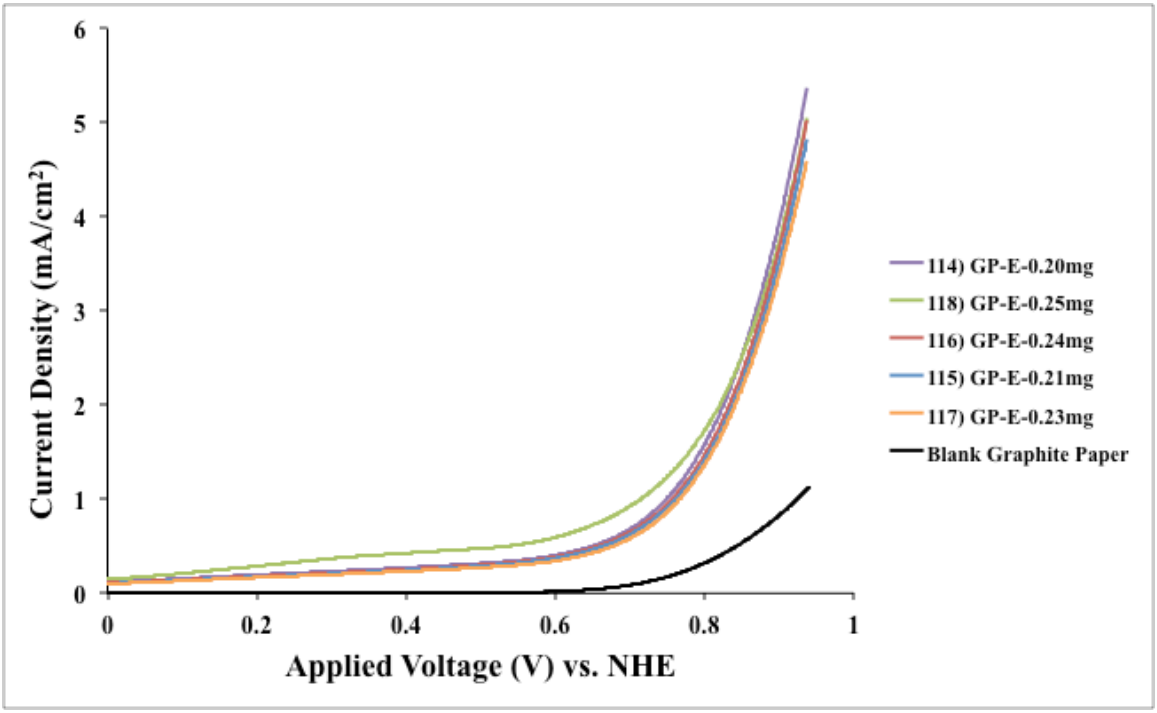

Figure 4.25: Electrocatalytic activity of EPD deposits at a constant deposition time of 2 minutes and a constant deposition current of 10 mA on graphite paper substrates in 2 M ammonium sulfite

Table 4.13: Deposit weight and electrochemical data for EPD on carbon felt (2 cm^2 deposition area) at a deposition current of 8 mA and deposition time of 30 seconds

Sample Number	Deposited Weight (mg)	Current Density (mA/cm^2)*
Blank	0.00	20.3
214	0.22	93.0
215	0.27	82.4
216	0.23	85.5
217	0.19	87.0
218	0.24	82.1

*Current density measurements taken at an applied voltage of 0.9

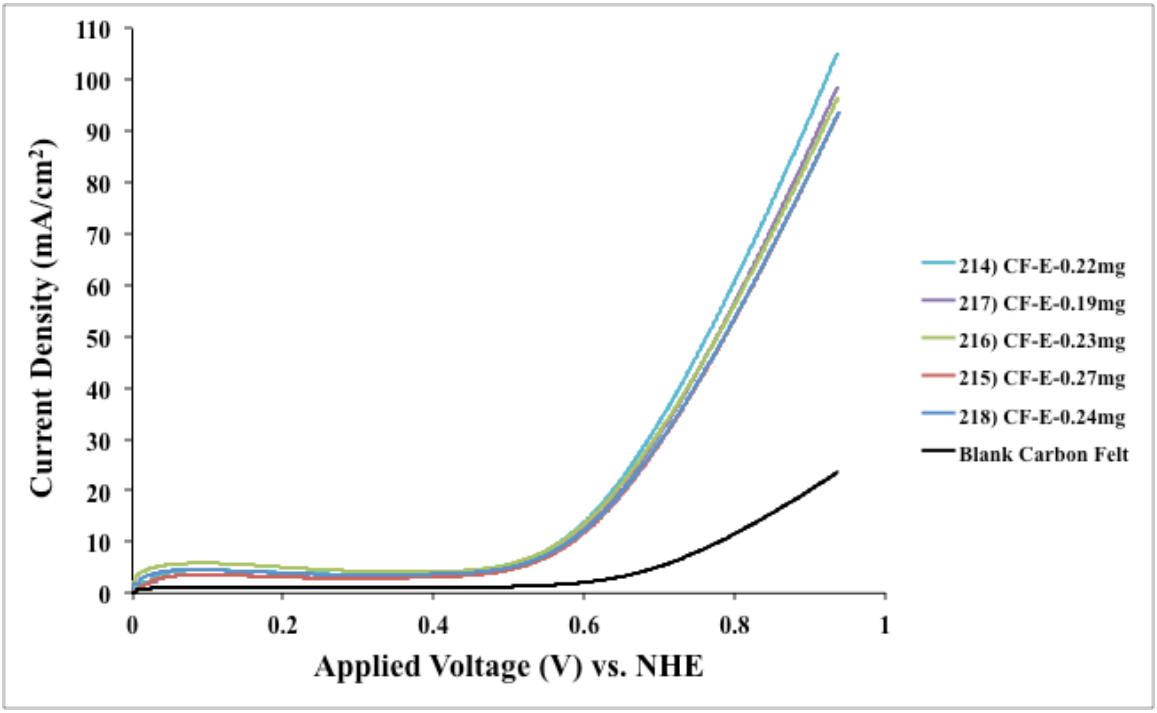

Figure 4.26: Electrocatalytic activity of EPD deposits at a constant deposition time of 30 seconds and a constant deposition current of 8 mA on carbon felt substrates in 2 M ammonium sulfite

References

[1] Pacheco, N.S. Electrophoretic Deposition of Cobalt Ferrite Nanoparticles into 3D Felt. M.S. Thesis, University of California, San Diego, 2015.

Chapter 5. Conclusions and Future Work

The primary motivation of this study was to help in the development of a cost-effective means of producing hydrogen through a SA thermochemical cycle. In order to achieve this goal, cobalt ferrite nanoparticles were analyzed as an economical alternative to platinum-based catalysts for the hydrogen-producing electrolyzer. EPD of the nanoparticles was performed on various substrates to study the influence of deposition conditions on deposit morphologies. Subsequently, linear sweep voltammetry and SEM analyses were performed to explore the effects of deposit morphology on overall electrochemical activity of the deposits. EPD conditions that resulted in thin deposit films were of particular interest, as it was sought to minimize the amount of catalyst needed while exposing the nanoparticles for maximum activity.

Experiments showed that EPD on graphite paper at a deposition current of 10 mA and deposition time of 2 minutes produced the most electrochemically active results of all graphite paper deposits. Under these conditions, the deposit tested 5.5 times better than a blank graphite paper substrate. Moreover, its current density was roughly 56% of its platinum cobalt comparison, at an applied voltage of 0.9 V. It was estimated that there were 3 cobalt ferrite nanoparticle layers present on this graphite paper deposit. SEM analysis showed that the deposit was thick enough to induce cracking.

Electrophoretic deposition on carbon felt at a deposition current of 8 mA and deposition time of 30 seconds produced the most electrochemically active results from all carbon felt deposits. For these conditions, the deposit tested 4.3 times better than a blank carbon felt substrate. Furthermore, its current density was approximately 58% of its

platinum cobalt comparison, at an applied voltage of 0.9 V. It was estimated that there were roughly 0.13 particle layers present throughout the deposit. SEM images from the outer surface of the sample showed a uniform, thin deposit film. However, images at the middle of the sample showed regions of exposed substrate, suggesting that the particles did not completely penetrate the carbon felt and deposit uniformly throughout.

In order to see if the findings in this thesis can be applied to a full-scale industrial process, future work should include analysis of the scalability of this research. Additionally, further work should expand on the EPD conditions studied in this research. Such work should include analysis of different deposition times, deposition currents, and particle suspension concentrations. Furthermore, experiments using different bath chemistries should be performed under the same deposition conditions presented in this research for comparison.

Appendix

Product Name: **Certificate of Analysis**

Platinum cobalt on carbon – extent of labeling: 30 wt. % Pt_3Co loading

Product Number:	**738565**
Batch Number:	**MKBJ0577V**
Brand:	ALDRICH
Formula:	CoPt3
Quality Release Date:	20 OCT 2011

Pt_3Co

Figure A.1: Platinum cobalt nanoparticle information [1]

	GF-S2
Type	Carbon Fiber Paper
Fiber Density	0.063 lbs/in^3
Paper Areal Weight	1.0 oz/yd^2
Paper Surface Resistivity	< 10Ω per square
Paper Thickness	14 mil
Paper Tensile strength	10 lb/in
Binder content	10%

Figure A.2: Graphite paper specifications

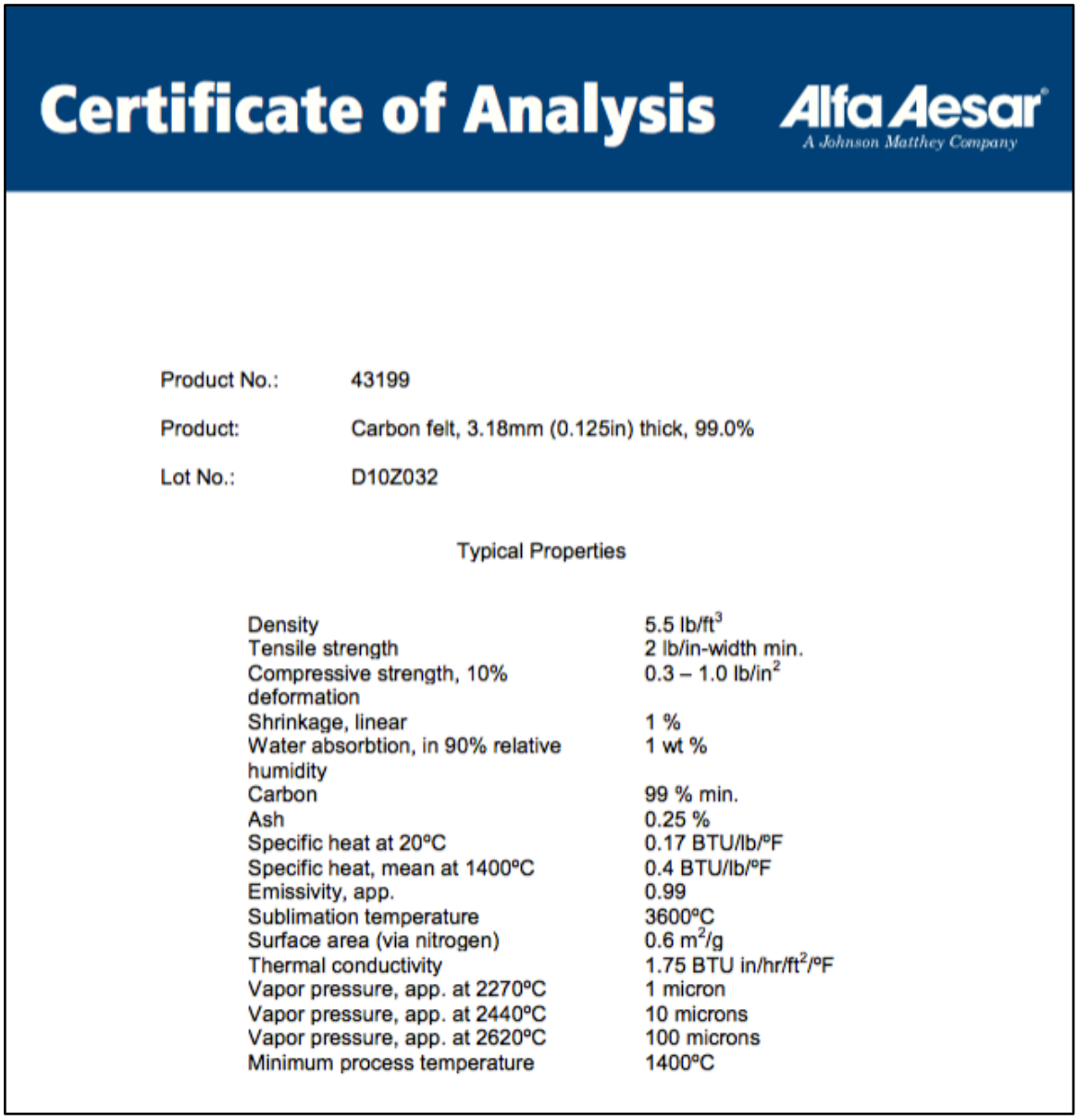

Certificate of Analysis

Alfa Aesar
A Johnson Matthey Company

Product No.: 43199

Product: Carbon felt, 3.18mm (0.125in) thick, 99.0%

Lot No.: D10Z032

Typical Properties

Density	5.5 lb/ft^3
Tensile strength	2 lb/in-width min.
Compressive strength, 10% deformation	0.3 – 1.0 lb/in^2
Shrinkage, linear	1 %
Water absorbtion, in 90% relative humidity	1 wt %
Carbon	99 % min.
Ash	0.25 %
Specific heat at 20°C	0.17 BTU/lb/°F
Specific heat, mean at 1400°C	0.4 BTU/lb/°F
Emissivity, app.	0.99
Sublimation temperature	3600°C
Surface area (via nitrogen)	0.6 m^2/g
Thermal conductivity	1.75 BTU in/hr/ft^2/°F
Vapor pressure, app. at 2270°C	1 micron
Vapor pressure, app. at 2440°C	10 microns
Vapor pressure, app. at 2620°C	100 microns
Minimum process temperature	1400°C

Figure A.3: Carbon felt substrate specifications [2]

References

[1] Sigma Aldrich. *Platinum cobalt on carbon*; http://www.sigmaaldrich.com/catalog/product/aldrich/738565?lang=en&region=US, Product No. 738565.

[2] Alfa Aesar. *Carbon felt*; https://www.alfa.com/en/catalog/043199/, Product No. 43199.